Abstract Spectral line-by-line shaping is a key enabler towards optical arbitrary waveform generation, which promises broad impact both in optical science and technology. In this paper, generation of optical and microwave arbitrary waveforms using the spectral line-by-line shaping technique is reviewed. Compared to conventional pulse shaping, significant new physics arises in the line-by-line regime, where the shaped pulse fields generated from one laser pulse now overlap with those generated from adjacent pulses. This leads to coherent interference effects related to the properties of optical frequency combs which serve as the source in these experiments. We explore such effects in a series of experiments using several different high-repetition-rate optical combs, including harmonically mode-locked lasers and continuous-wave lasers that are externally phase modulated either with or without the help of an optical cavity. As an application of line-by-line pulse shaping, we describe generation of microwave electrical arbitrary waveforms that can be reprogrammed at rates approaching 10 GHz.

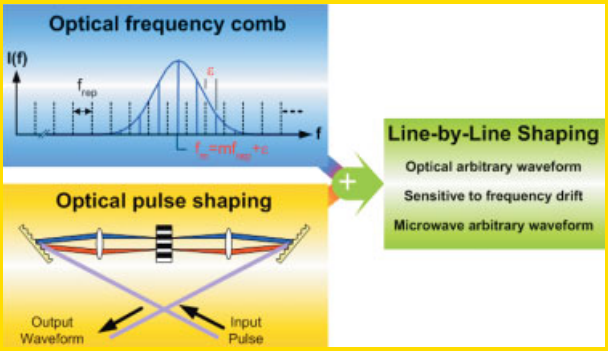

Significance of line-by-line shaping: combining optical frequency combs with spectral pulse shaping

Spectral line-by-line shaping for optical and microwave arbitrary waveform generations

Chen-Bin Huang [1,2], *Zhi Jiang* [1,3], *Daniel E. Leaird* [1], *José Caraquitena* [1,4], *and Andrew M. Weiner* [1,*]

[1] School of Electrical and Computer Engineering, Purdue University, West Lafayette, IN 47907-2035, USA
[2] Current address: Bell Laboratories, Alcatel Lucent, Murray Hill, NJ 07974, USA
[3] Current address: Beckman Institute, University of Illinois at Urbana-Champaign, Urbana, IL 61801, USA
[4] Current address: Nanophotonics Technology Center, Universidad Politécnica de Valencia, 46022 Valencia, Spain

Received: 4 February 2008, Revised: 17 March 2008, Accepted: 17 March 2008
Published online: 23 April 2008

Key words: Optical pulse shaping; signal processing; optical fiber communications; ultrafast processing

PACS: 42.30.Kq, 42.62.-b, 42.65.Re

1. Introduction

Optical pulse shaping is a widely adopted technique, in which intensity and phase manipulation of optical spectral components allows synthesis of user-specified ultrashort pulse fields according to a Fourier transform relationship [1]. As shown in Fig. 1, the most commonly used shaper geometry uses a grating to map the frequency components of the input pulse onto space. Optical pulse shaping has enabled various applications, such as optical pulse compression, shaped wave optical communication systems, spectrally selective nonlinear microscopy, and quantum coherent control just to name a few. On the other hand, mode-locked lasers producing combs of frequency stabilized spectral lines have resulted in revolutionary advances in frequency metrology [2], extremely high precision spectroscopy [3, 4], and high-sensitivity real-time gas detection [5]. Some applications of the fields overlap, such as radio-frequency photonics [6] and LIDAR [7]. However, until recently pulse shapers addressed spectral lines in groups at low spectral resolution. Line-by-line pulse shaping [8], in which spectral lines are resolved and manipulated individually, leads to a fundamentally new regime for optical arbitrary waveform generation (O-AWG) [9, 10], in which the advantages of pulse shaping and of frequency combs are exploited simultaneously.

* Corresponding author: e-mail: amw@ecn.purdue.edu

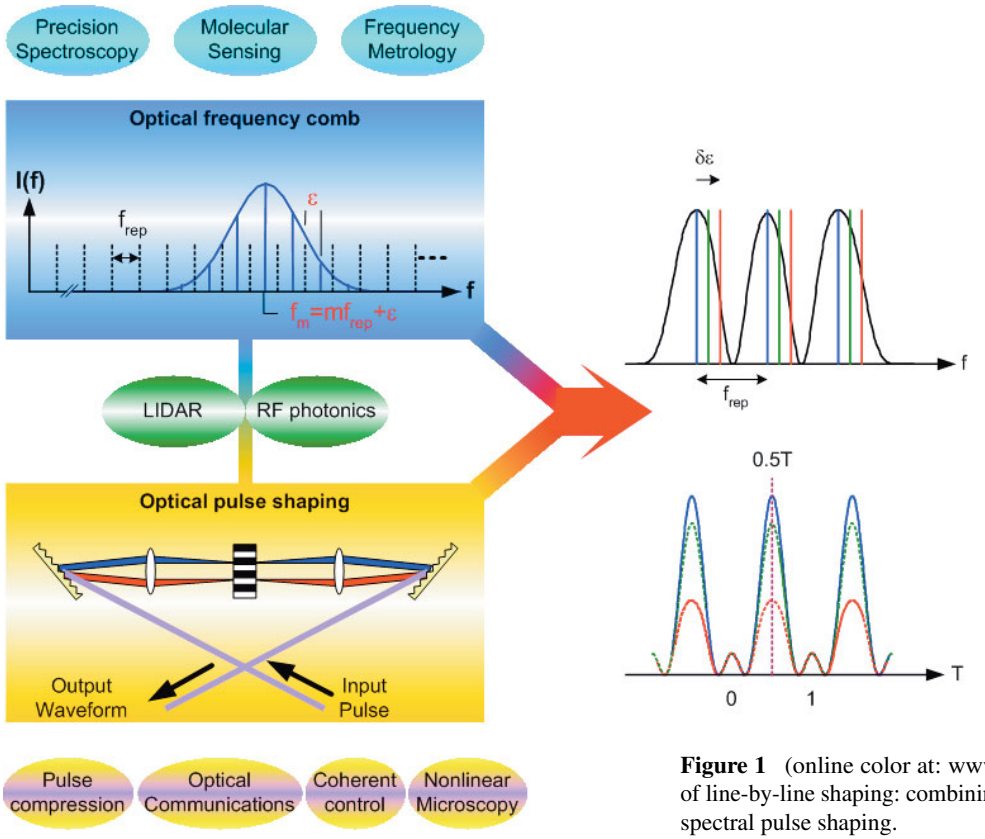

Figure 1 (online color at: www.lpr-journal.org) Significance of line-by-line shaping: combining optical frequency combs with spectral pulse shaping.

Furthermore, significant new physics arises in line-by-line shaping, where the shaped pulse fields generated from one laser pulse now overlap with those generated from adjacent pulses. In this situation the overall waveform inherently depends on the interference between contributions from different laser pulses. This interference in turn is sensitive to the relative phase of different pulses of the comb, which is directly related to the optical comb offset frequency. In this way, line-by-line shaping unites the key concepts of pulse shaping with those of frequency combs.

Bringing pulse shaping and frequency combs together allows O-AWG with both controllable ultrafast time structure and long term coherence. Intuitively, full control of individual frequency comb lines require: (1) frequency stabilized sources to generate stable spectral lines; (2) high resolution pulse shapers to resolve and control individual spectral lines. Combining pulse shaping and frequency combs should lead to new applications drawing on both technologies. O-AWG promises broad impact both in optical science, allowing for example coherent control generalizations of comb-based time-frequency spectroscopies, and in technology, enabling new truly coherent multi-wavelength processing concepts for spread spectrum lightwave communications and LIDAR.

This review is organized as follows: In the second section, we discuss the relation of line-by-line pulse shaping to conventional pulse shaping. The experimental setup that enables line-by-line pulse shaping is also described. Some fundamental demonstrations of spectral line-by-line shaping performed using an active harmonically mode-locked fiber laser source will be presented in the third section. One issue with such a source is relatively poor optical frequency stability, which enters into pulse shaping in the line-by-line regime in a fundamental way. The new effects of frequency comb frequency instabilities in line-by-line shaping are explored in the fourth section. In the fifth section, pulse shaping examples using alternative comb sources are also demonstrated. In particular, here we discuss line-by-line shaping for compression and manipulation of combs generated via phase modulation, either with or without the aid of an optical cavity. Such sources provide us improved frequency stability compared to the high repetition rate harmonically mode-locked laser used in the experiments of earlier sections. In section six, we discuss an exciting new application of line-by-line shaping – namely, arbitrary ultrawideband microwave waveform generation with waveform programmability as fast as 10 GHz rate. This capability is not offered by any of today's electronic waveform generation solutions. The last section provides conclusions.

2. Line-by-line shaping and shaper setup

Previous pulse shapers have generally manipulated groups of spectral lines rather than individual lines, which results in waveform bursts that are separated in time with low duty

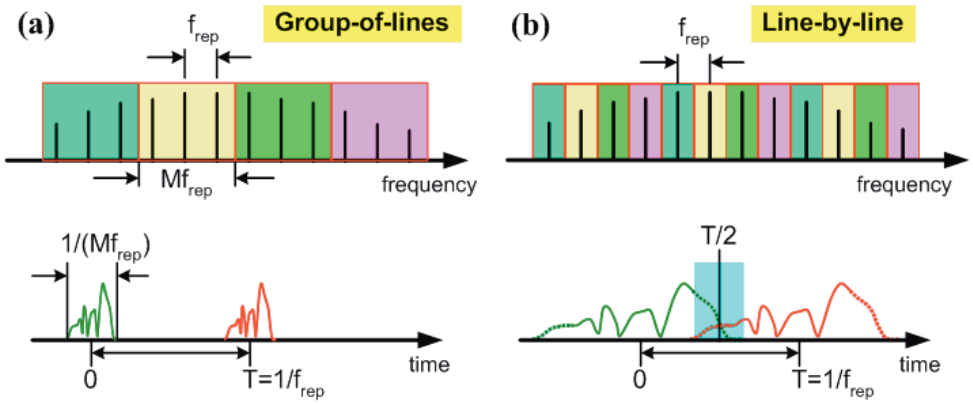

Figure 2 (online color at: www.lpr-journal.org) Illustration of pulse shaping with (a) group of lines and (b) line-by-line regime.

factor which are insensitive to the absolute frequency positions of the mode-locked comb. This is primarily due to the practical difficulty of building a pulse shaper capable of resolving each spectral line for typical mode-locked lasers with repetition rates below 1 GHz. When extending pulse shaping to independently manipulate the intensity and phase of individual spectral lines (line-by-line pulse shaping), the shaped pulses can overlap with each other, which leads to waveforms spanning the full time period between mode-locked pulses (100% duty factor). Waveform contributions arising from adjacent mode-locked pulses will
to the offset of the frequency comb [8]. Such line-by-line control is an important step towards O-AWG since the intensity and phase of each individual spectral line is independently controlled. Previous efforts towards spectral line-by-line control utilized a hyperfine filter but were limited within a narrow optical bandwidth - the free spectral range of this device [9]. Recently, we demonstrated spectral intensity/phase line-by-line pulse shaping [8] and thus O-AWG over a considerably broader band [10] based on high resolution grating-based pulse shapers.

Group-of-lines pulse shaping is illustrated in Fig. 2(a), where f_{rep} is the spacing between comb lines. Assuming that the pulse shaping occurs M lines at a time, the shaped pulses have maximum duration $1/(M f_{\text{rep}})$ and repeat with period $T = 1/f_{\text{rep}}$. Accordingly, the pulses are isolated in time. In contrast, for line-by-line pulse shaping ($M = 1$), as shown in Fig. 2(b), the shaped pulses can overlap, which leads to interference between contributions from different input pulses in the overlapped region. Previously, a hyperfine wavelength-division multiplexing filter was used for spectral line-by-line phase manipulation with 5 GHz line spacing in an optical code division multi-access system and with 12.4 GHz spacing in photonic RF arbitrary waveform generation experiments [9] but without investigation of this pulse overlap issue. More importantly, the hyperfine wavelength-division device has a periodic spectral response, which means that independent manipulation of the spectrum is possible only within one free spectral range, which was only 75–80 GHz in the experiments described in [9].

Our free-space grating-based shaper setup is illustrated in Fig. 3. A fiber-pigtailed collimator and subsequent telescope take the light out of fiber and magnify the beam size to ~ 18 mm diameter on the 1200 grooves/mm grating in order to increase the pulse shaper resolution. A fiberized polarization controller is used to adjust for horizontal polarization on the grating. A polarization beam splitter (PBS) aligned for horizontal polarization is inserted between the collimator and the telescope. Discrete comb lines are diffracted by the grating and focused by a lens with 1000 mm focal length. The spectral resolution of our

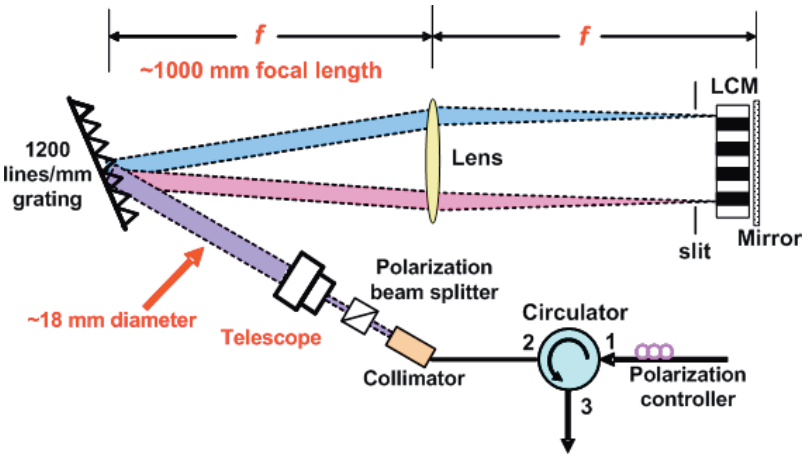

Figure 3 (online color at: www.lpr-journal.org) Schematic of a reflective line-by-line shaper. LCM: liquid crystal modulator.

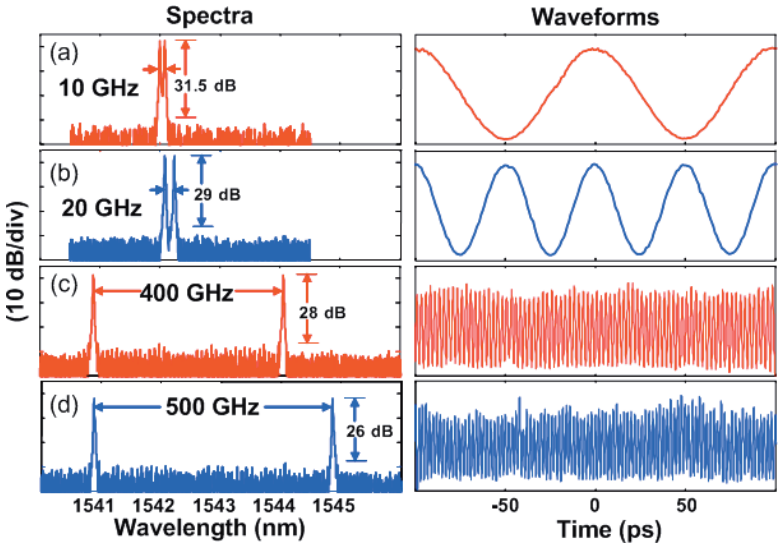

Figure 4 (online color at: www.lpr-journal.org) Selecting two spectral lines (separated by a: 10 GHz, b: 20 GHz, c: 400 GHz and d: 500 GHz) and corresponding cosine waveforms (with periods of 100 ps, 50 ps, 2.5 ps and 2 ps). Waveforms for (a,b) are measured using a sampling scope while (c,d) using cross-correlation.

shaper is 2.6 GHz. A 2×128 pixel liquid crystal modulator (LCM) array is placed just before the lens focal plane to independently control both amplitude and phase of individual spectral lines. The LCM in our experiment is fully integrated with control electronics and software. A gold mirror is placed at the minimum focusing plane, leading to a double-pass geometry, with all the spectral lines recombined into a single fiber and separated from the input via an optical circulator. Amplitude manipulation is realized by LCM control and the polarization extinction of the PBS in the recombination path back into the collimator. A pair of razor blades placed just before the LCM can be used as a width-tunable slit for better optical extinction ratio. The total optical loss is around 10 dB. We note that in addition to LCMs, other spatial light modulators are also well-known in pulse shaping [1]. Line-by-line pulse shaping experiments analogous to those reported here should also be possible using other spatial light modulator technologies, provided that the key requirement of very high spectral resolution for clear separation of adjacent spectral lines is met.

3. Line-by-line shaping using mode-locked lasers

3.1. Optical and RF arbitrary waveform generation

In this section we show shaping examples performed using a home-built harmonically mode-locked fiber laser producing 3 ps (full width at half maximum) pulses at 9-10 GHz tunable repetition rates with a center wavelength of 1542.0 nm [10]. The repetition rate, selected to ensure that the spectral line spacing exceeds the pulse shaper resolution, is especially appropriate for practical applications in optical communications. Each spectral line is spaced by 200 μm, corresponding to 2 LCM pixels. The frequency offset of the mode-locked comb is not actively stabilized; instead we exploit the passive frequency stability of the mode-locked comb, ~ 1 GHz over the time scale of our experiments (ten times below the comb spacing). The comb frequency instability was determined by heterodyne beating with a continuous-wave laser with 15 MHz linewidth over one minute. This suffices for these first proof-of-concept experiments on line-by-line pulse shaping control for O-AWG under typical laboratory environmental conditions without additional controls (e.g., temperature stabilization). However, note that in line-by-line shaping, optical frequency noise is converted to time-domain waveform intensity noise. This phenomenon is fundamentally new to line-by-line shaping and does not occur in group-of-line shaping regime. Some discussion is given in Sect. 4.

To achieve a larger number of spectral lines, the 3 ps pulses are compressed to 400 fs by a commercially available dispersion-decreasing fiber soliton compressor. Either 3 ps or 400 fs pulses at 10 GHz repetition rate are used as input to the pulse shaper according to the required bandwidth for the specific demonstration.

Fig. 4 shows power spectra (log scale) and resulting time-domain intensity waveforms when the pulse shaper is used to select just two spectral lines out of the mode-locked frequency comb. Data are shown for spectral line separations of 10 and 20 GHz (Fig. 4(a-b), 3 ps input pulses) and 400 and 500 GHz (Fig. 4(c-d), 400 fs input pulses). The measured optical linewidths are limited by the 0.01 nm resolution of the optical spectrum analyzer. The log plots reveal that deselected spectral lines are suppressed by greater than 31.5 dB for 10 GHz, 29 dB for 20 GHz, 28 dB for 400 GHz, and 26 dB for 500 GHz. The intensity waveform resulting from selection of two spectral lines is ideally a cosine function with DC offset. Data shown in the figures reveal cosines with periods of 100, 50, 2.5, and 2 ps, respectively, as expected. These data are measured after an optical amplifier, using either a 50 GHz bandwidth photodiode and

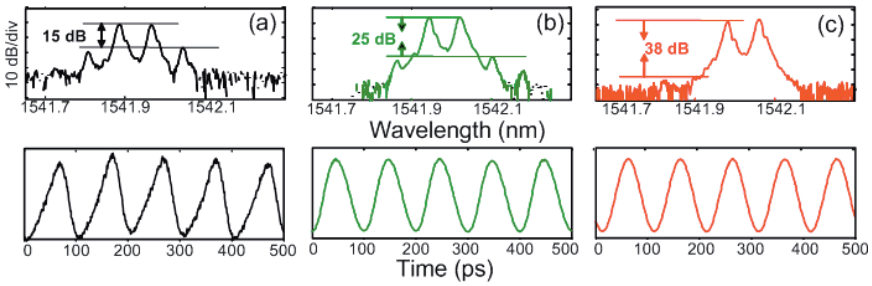

Figure 5 (online color at: www.lpr-journal.org) Waveforms with suppression ratios of the deselected lines: (a) 15 dB, (b) 25 dB and (c) 38 dB.

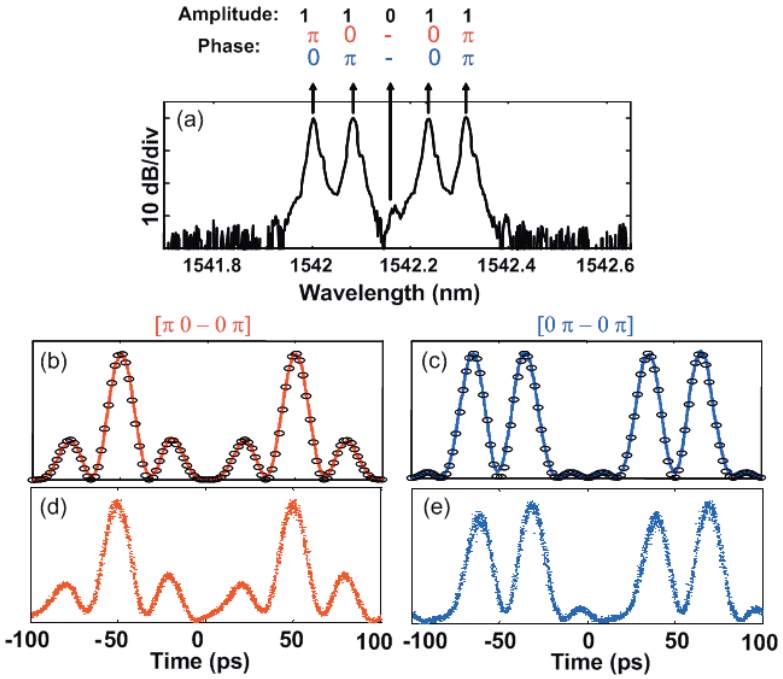

Figure 6 (online color at: www.lpr-journal.org) (a) Selecting four spectral lines (five consecutive lines with center line blocked). (b,c) Waveforms measured by intensity cross-correlation with different applied spectral phases (red and blue curves). Calculations (black circles) are essentially indistinguishable from the data, showing the high fidelity of the generated waveforms. (d,e) Waveforms are detected by a 50 GHz photo-diode and measured by sampling scope in persistent mode to demonstrate radio frequency arbitrary waveform generation (RF-AWG).

sampling scope (10 and 20 GHz) or standard short optical pulse intensity cross-correlation techniques (400 and 500 GHz). The pulse shaper itself is able to afford much higher frequency cosine waveforms, but here we are limited by the available optical bandwidth from the laser and by the measurement process (shorter reference pulses are required to measure higher frequency cosine waveforms with shorter period). This limitation can be relaxed by utilizing short pulse compression techniques to achieve large bandwidth at high repetition rate [10]. The increased fluctuations and distortions in the cosine waveforms at higher frequencies (especially 400 and 500 GHz) arise due to decreased optical power as the selected lines approach the edge of the input spectrum (10 μW optical power for the two lines with 500 GHz separation), which increases susceptibility to imperfect suppression of deselected lines and optical amplifier noise. Nevertheless, these data clearly demonstrate the potential to synthesize modulations over a very broad frequency range.

It is essential to note that strong suppression of deselected spectral lines is critical for accurate waveform generation. To validate this point, Fig. 5 shows the two-line selection waveforms viewed on a sampling scope with different suppression ratios of the deselected lines. In Fig. 5(a), the waveform evidently deviates from a cosine function with only 15 dB of suppression ratio. For suppression ratio of 25 and 38 dB, the scope traces reveal a better cosine waveform in Fig. 5(b,c), respectively.

Fig. 6 shows another example of line-by-line pulse shaping control for O-AWG that highlights the fidelity of our method. Four spectral lines (five consecutive lines with the center line blocked, Fig. 6(a)) are selected within a relatively narrow bandwidth to ease comparison with a theoretical calculation. By applying the same amplitude modulation ($[1\ 1\ 0\ 1\ 1]$) but different phase modulation ($[\pi\ 0\ -\ 0\ \pi]$ or $[0\ \pi\ -\ 0\ \pi]$), two distinct waveforms are generated. The intensity cross-correlation measurements are in almost perfect agreement with the calculations (black circles) based on the Fourier transform of the nominal amplitude and phase patterns imparted onto the spectral lines (Fig. 6(b-c)). The key point is that one can now synthesize high fidelity optical waveforms with desired amplitude and phase with 100% duty factor, by manipulating the individual spectral lines from a mode-locked frequency comb. It should also be noted that to clearly illustrate the relationship between the time and frequency domains, intensity

Figure 7 (online color at: www.lpr-journal.org) Schematic of temporal Talbot effect.

and phase control are demonstrated in a binary fashion. As is well known, both intensity and phase gray level control can be readily achieved [1, 8, 11] using a LCM. The comb lines shown in Fig. 6(a) are intensity equalized in this demonstration.

One immediate application of line-by-line pulse shaping is for radio-frequency arbitrary waveform generation (RF-AWG). Fig. 6(d-e) show sampling scope measurements of the electrical output generated when the optical waveforms of Fig. 6(b-c) drive a 50 GHz photo-diode. Such highly structured broadband radio-frequency waveforms are impossible to implement using current electrical AWG technology which is typically limited to $\sim$ 1 GHz [12]. The slight distortions of the RF waveforms compared with the driving optical signals are caused by the limited bandwidth of the photodiode and the sampling scope, which could be pre-compensated (for example, to achieve two equal main peaks in Fig. 6(e)) by appropriately modifying the control signals to the optical driving waveforms. RF-AWG has the potential to impact fields such as ultra-wideband (UWB) wireless [13], which uses sub-nanosecond electrical bursts for communications and sensing, and impulse radar, where the use of highly structured transmit waveforms designed to optimize discrimination between different scattering targets has been proposed [14].

3.2. Pulse repetition-rate multiplication

Optical pulse trains with high repetition rates are very attractive for ultrahigh-speed optical communication systems and signal processing. Recently, several research groups have been exploring techniques for generating periodic pulse trains at repetition rates beyond those achievable by mode locking or direct modulation. One alternative is repetition-rate multiplication (RRM) of a lower rate source by applying amplitude [15–17] or phase [18–20] spectral filtering. A technique based on the temporal Talbot effect [21] is a simple and efficient method, as it simply requires the propagation of the pulse train in a first-order dispersive medium. This technique, equivalent to a phase-only filtering process, has been traditionally demonstrated by using conventional optical fibers [18, 19] or linearly chirped fiber Bragg gratings [20]. Here we demonstrate high-quality repetition-rate multiplication based on line-by-line shaping on a 9 GHz actively mode-locked fiber laser [22].

Fig. 7 illustrates the temporal Talbot effect for RRM [21]. This phenomenon occurs when periodic trains of optical pulses propagate through a first-order dispersive medium. An appropriate amount of dispersion leads either to reproduction of the original pulse train (integer temporal Talbot effect) or repetition-rate multiplication by an integer factor (fractional temporal Talbot effect). For our purposes it is important to note that it is unnecessary to introduce continuous first-order dispersion.

In fact, only the spectral phases at frequencies equal to the discrete spectral lines, $\omega_n = \omega_0 + n\omega_{\text{rep}}$, are relevant, where ω_0 is the carrier frequency, ω_{rep} is the input repetition rate, and n is an integer. The Talbot condition [21] provides the phase shifts that must be applied to the different spectral lines to obtain repetition-rate multiplication:

$$\phi(\omega_n) = \frac{s}{r}\pi n^2 \qquad (1)$$

where s and r are mutually prime integer numbers. The multiplication factor is given by the integer r. Maximum repetition-rate multiplication is limited by the input pulse duration, which must be short enough to prevent pulse overlapping in the multiplied train. In practice, the actual phase shifts are applied by the pulse shaper modulo 2π, which yields a periodic phase filter [23, 24], as shown in Fig. 8.

Initially, the generated trains with multiplied repetition-rate show significant peak-to-peak pulse intensity variations. We attribute this undesired effect to small phase errors in the calibration of the LCM and to weak cross-talk between adjacent spectral lines due to the finite spectral resolution. To obtain uniform pulse intensities, we use an iterative correction algorithm that adaptively modifies the phases applied by the LCM. The algorithm starts with the phase sequence $\{\phi_0, \phi_1, \phi_2, \ldots \phi_N\}$, obtained from Eq. (1). Next, the first phase ϕ_0 is modified, $\phi_0' = \phi_0 \pm \varepsilon$, with ε a preset phase error, and the resultant output trains are measured. The algorithm selects the new phase ϕ_0' that generates the output train with smallest peak-to-peak pulse intensity variation. Next, a similar procedure is applied sequentially for

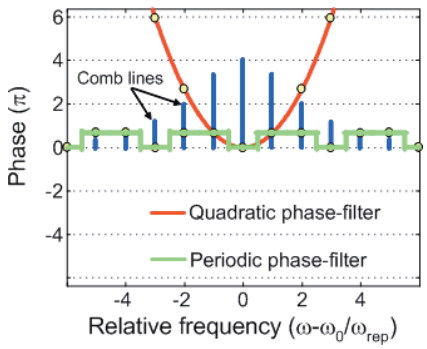

Figure 8 (online color at: www.lpr-journal.org) Talbot filter function. Periodic phase filter is applied in line-by-line shaping.

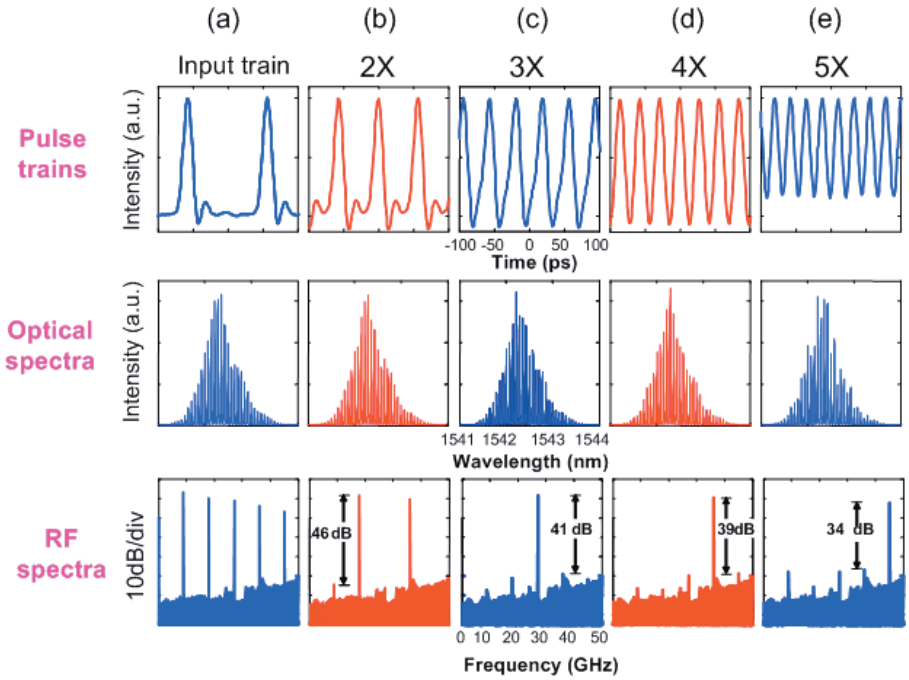

Figure 9 (online color at: www.lpr-journal.org) Experimental results of pulse repetition-rate multiplication using phase-only filtering.

the second and other phases in the sequence, finally obtaining a new series of phase values $\{\phi_0^{'}, \phi_1^{'}, \phi_2^{'}, \ldots \phi_N^{'}\}$. For some of the multiplication factors, namely, three-to-five-times repetition-rate multiplication, we also used a similar procedure to adjust the spectral amplitudes. We iteratively repeated this procedure, while decreasing the value of ε from one iteration to the next. Typically five or six iterations were required to minimize peak-to-peak pulse intensity variations in the output pulse train. The rms (maximum) spectral phase and intensity changes imposed by the algorithm were 0.076 rad (0.135 rad) and 7.5% (15%), respectively. These small changes were found to have quite a significant effect on the quality of the output pulse trains (see below), thus underscoring the need for high accuracy in Talbot effect experiments and the benefit of the fine-tuning capability in the apparatus.

In Fig. 9 (top row), we show experimental oscilloscope traces both for the unfiltered pulse train and for the multiplied trains at 18, 27, 36, and 45 GHz, respectively, obtained after applying the iterative correction algorithm. The multiplied trains now have very low peak-to-peak pulse intensity variations. In particular, we obtain $\sim 1\%$, 1.5%, 1.5%, and 2% maximum peak-to-peak variations for the 18, 27, 36, and 45 GHz output trains, respectively. In general, we are able to routinely generate multiplied trains with less than 3% peak-to-peak pulse intensity variations. In Fig. 9 (middle row), we show the optical spectra of the fundamental and multiplied pulse trains. All spectra are very similar which confirms that the technique is based on a phase-only filtering process. For comparison, we must mention that tunable pulse repetition-rate multiplication experiments in which the temporal Talbot effect was implemented by using dispersive fibers [25] and linearly chirped fiber Bragg gratings [26] yielded multiplied trains with significantly larger intensity variations in the range (8%–17%) and (7%–17%), respectively. We note here that the temporal Talbot effect multiplies only the pulse intensity repetition-rate, but not the temporal phase repetition-rate [21]. However, this method can be combined with other schemes to obtain real repetition-rate multiplication [27]. Further, it is also possible to multiply the repetition rate by performing spectral selection [15, 16] with our line-by-line shaper as an amplitude filter.

To further illustrate the high degree of uniformity we have achieved, RF spectrum analyzer measurements of the multiplied pulse trains are also plotted in Fig. 9 (bottom row). For the original pulse train (without spectral filtering), RF tones at 9 GHz and its harmonics are observed, as expected. When the pulse shaper is programmed for two-times multiplication, Fig. 9(b), the now undesired tones at 9 and 27 GHz are suppressed almost into the noise floor, 46 dB below the 18 GHz tone. This large suppression factor is consistent with the degree of intensity variation from the scope traces. Figs. 9(c)-(e) depict the RF spectra of the multiplied trains at 27, 36, and 45 GHz, respectively. Relative to the desired tone at the multiplied repetition rate, the undesired tones are suppressed by 41, 39, and 34 dB, respectively. Much of the slight reduction in suppression ratio with increasing repetition rate can be explained due to the roll-off of our measurement system at higher frequencies.

Our experimental demonstration of periodic spectral phase filtering implemented via line-by-line pulse shaping produces excellent two-to-five-times RRM of a 9 GHz mode-locked laser. Higher repetition-rate multiplication factors can be readily achieved if trains with shorter pulses are used as the input. This experiment also illustrates the ability of our high resolution pulse shaper to perform simultaneous, accurate, and independent programmable control of

individual spectral lines over the whole optical bandwidth of the mode-locked laser. As a result, we have achieved unprecedented uniformity in pulse trains multiplied according to the temporal Talbot effect.

3.3. Optical arbitrary pulse train generation

Among the almost arbitrary waveforms enabled by pulse shaping, a subset with particular appeal involves generation and manipulation of optical pulse trains. The simplest examples for continuous pulse train operation are repetition rate multiplication (RRM), as we demonstrated in the earlier subsection, which are usually implemented by spectral intensity or spectral phase filtering. In addition to simple RRM, continuous pulse trains with controllable patterns and envelopes have also been proposed and demonstrated [28–30]. In these demonstrations, high repetition rate mode-locked lasers (~ 10 GHz) are essential. In the frequency domain the output of such mode-locked lasers are characterized by an evenly spaced series of discrete spectral lines, with the frequency spacing equal to the pulse repetition rate. In this subsection we demonstrate optical arbitrary pulse train generation (OAPTG) using spectral line-by-line pulse shaping, in which a pulse train spanning the whole period can be generated and individual pulses can be independently manipulated to have different user-specified waveforms [31]. This is in contrast to previous work on pulse train generation using Fourier transform pulse shapers in the group of lines pulse shaping regime [11, 32, 33], in which sequences of pulses with different shapes have been demonstrated, but only over a time aperture short compared to the repetition period. This limitation associated with the group of lines regime hinders capabilities for pulse train generation significantly, for example, even two-times RRM is impossible.

For the purpose of OAPTG, the filter function has to be obtained first in order to properly control the spectral components of short periodic input pulses with our Fourier transform line-by-line pulse shaper. Suppose the spectrum of the input pulses is $A(\omega)$, then $A(\omega)\cdot\exp(-i\omega\tau)$ corresponds to pulses with delay τ. Consider generating a simple pulse train with two identical unshaped pulses in each period, the spectrum is $A(\omega)+A(\omega)\cdot\exp(-i\omega\tau)$ and the resultant filter function is $H(\omega)=1+\exp(-i\omega\tau)$. This can be immediately generalized to a pulse train with many pulses in each period. Furthermore, individual pulses in each period can be shaped to desired waveforms in a different way. Mathematically, the filter function can be written as

$$H(\omega)=\sum_k a_k\exp(-i\omega\tau_k)\cdot H_k(\omega) \qquad (2)$$

where the complex amplitude a_k allows control of individual amplitudes and phases, the delay of the *k-th* pulse in the period is determined by τ_k and the waveform of the k-th pulse is determined by its individual filter function $H_k(\omega)$. It is clear that all pulses are phase coherent. In our following experiments, the required spectral intensity and phase control are derived from the filter function in Eq. (2). The spectral intensity control is normalized to the maximum of $|H(\omega)|^2$. The number of pulses is limited by the period and pulse width. In most of our experiments, the delays between pulses are sufficiently large, so pulses are well separated.

Our experiments are performed using a harmonically mode-locked fiber laser producing 3.5 ps (FWHM) pulses centered near 1542 nm. The laser is running at 9.15 GHz, which precisely maps the spectral line spacing of the laser to the pixel spacing of the pulse shaper (we use two pixels to control one spectral line). These short pulses are input into the line-by-line pulse shaper, which can be easily programmed to allow for convenient testing with various arbitrary optical pulse trains. The output of the pulse shaper is measured by an optical spectrum analyzer and intensity cross-correlator using the initial unshaped pulse as the reference.

Fig. 10(a) shows a pulse train with binary pattern $[1\ 1\ 0\ 1]$ in each period, where pulses are located at 0, $T/4$ and $3T/4$. Pulse intensities for '1' are very close to equal and are negligible for '0' (-25 dB lower). Both attributes still remain significant challenges in previous demonstrations [30]. To show arbitrary temporal intensity control rather than a binary pattern, an example of an intensity ladder pattern $[0\ \frac{1}{4}\ \frac{1}{2}\ 1]$ is presented in Fig. 10(b). Unlike simple RRM in Fig. 9 implemented by either a spectral intensity only or phase only filter function, the patterns in Fig. 10 generally require simultaneous spectral intensity and phase control. (Note however that the pattern $[1\ 1\ 0\ 1]$ can also be generated by a phase only filter, e.g., with phases $(0\ 0\ 2\arctan(\sqrt{2})\ 2\arctan(\sqrt{2})\ldots)$). Also note that in Fig. 10(a) and 10(b) the pulses are evenly spaced, at the same temporal positions as in four times RRM, which results in periodic filter functions (periodic every four spectral lines). This is evident in the measured spectra. Fig. 10(c) shows an example for arbitrary delay control in contrast to Fig. 10(a) and 10(b). Three pulses in each period are located at 0 ps, -25 ps and -75 ps, resulting in irregular pulse separations ($\Delta\tau_1 = 50$ ps, $\Delta\tau_2 = 25$ ps, $\Delta\tau_3 = 34.3$ ps). As a result, the filter function is not periodic any more, as clear from the spectrum in Fig. 10(c). These examples demonstrate the capability for arbitrary temporal intensity and delay control on individual pulses in each period.

In the above examples, all the pulses essentially keep the same profile as the input pulse. According to Eq. (2), pulses within a single period may also be controlled individually to have different user-specified waveforms. Fig. 11(a) shows an example of 3 pulses in each period with one pulse broadened. The temporal broadening is realized by applying an additional spectral quadratic phase on this pulse. Fig. 11(b) shows an example of 2 pulses in each period with an additional spectral cubic phase applied on one of the pulses. This pulse shows an oscillatory tail as expected which is a sign of spectral cubic phase. Fig. 11(c) shows an

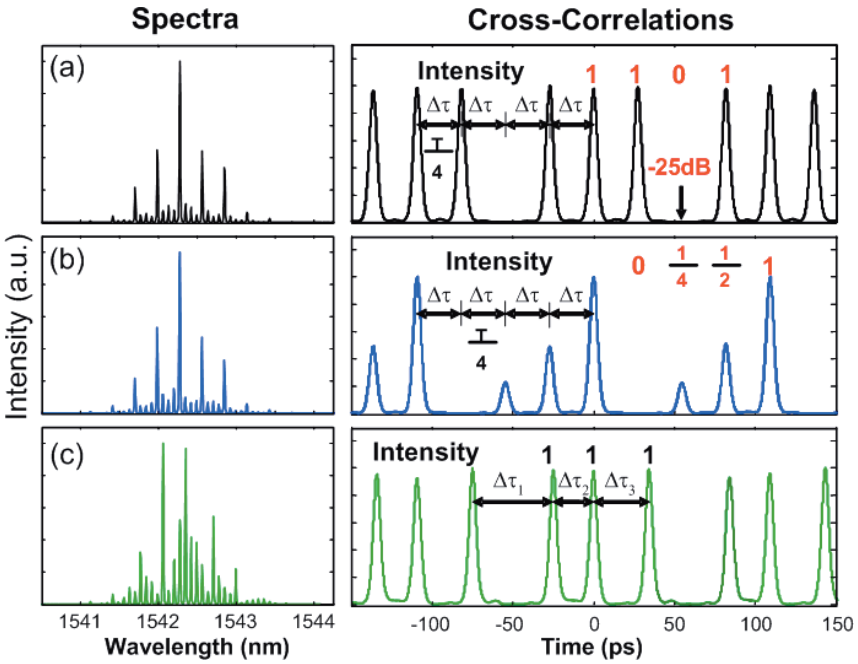

Figure 10 (online color at: www.lpr-journal.org) OAPTG examples. (a) Binary pattern [1 1 0 1]. (b) Ladder pattern [0 $\frac{1}{4}$ $\frac{1}{2}$ 1]. (c) Arbitrary delay ($\Delta\tau_1 = 50$ ps, $\Delta\tau_2 = 25$ ps, $\Delta\tau_3 = 34.3$ ps).

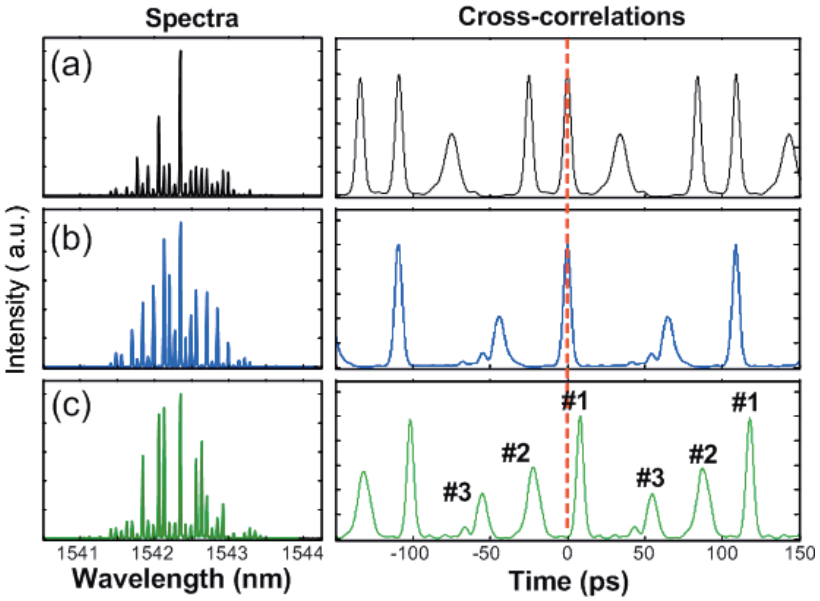

Figure 11 (online color at: www.lpr-journal.org) OAPTG examples. (a) One pulse width is broadened. (b) One pulse has spectral cubic phase. (c) Pulse #1 has spectral linear phase, pulse #2 has spectral quadratic phase, pulse #3 has spectral cubic phase.

example with 3 pulses in each period, where pulse #1 has a linear spectral phase (corresponding to temporal delay), pulse #2 has a quadratic spectral phase (corresponding to temporal broadening), pulse #3 has a cubic spectral phase (corresponding to an oscillatory temporal tail). These examples show the capability for OAPTG using line-by-line pulse shaping, in particular, the capability for achieving arbitrary waveform control on individual pulses in each period.

In the current scalar OAPTG experiments where we are concerned with only one polarization, the intensity control in our pulse shaper is obtained through polarization control together with a polarizer at the output [1, 11]. Therefore, we anticipate that vector OAPTG with the additional feature of polarization control can be readily achieved with minor modifications, similar to polarization pulse shaping experiments that have been reported in the group of lines regime [34–37].

3.4. Tunable optical RZ-to-NRZ format conversion

Return-to-zero (RZ) pulses have been widely used in optical fiber communication systems and optical networks, including RZ format transmission, soliton systems, optical

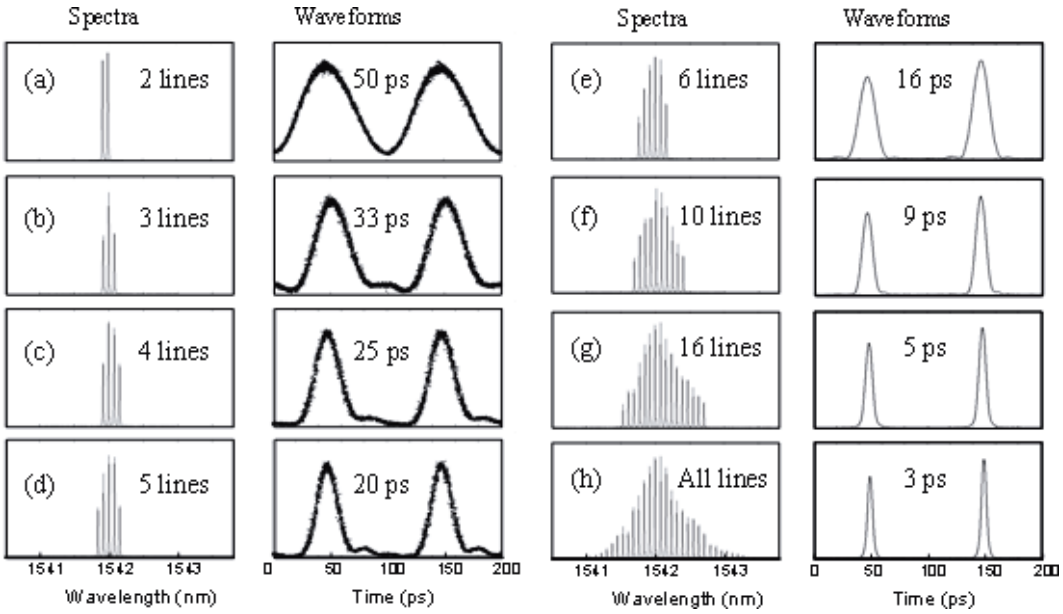

Figure 12 Line-by-line controlled spectra (linear scale) and waveforms, where the laser center wavelength is tuned to 1542 nm. The spectra are controlled to have (a) 2 lines, (b) 3 lines, (c) 4 lines and (d) 5 lines. These waveforms are detected by a 50 GHz photo-diode and sampling scope, showing tunable width of 50 ps, 33 ps, 25 ps and 20 ps, respectively. The spectra are controlled to have (e) 6 lines, (f) 10 lines, (g) 16 lines and (h) all lines. These waveforms are measured by intensity cross-correlation measurements, showing tunable width of 16 ps, 9 ps, 5 ps and 3 ps after de-convolution, respectively.

time-division-multiplexing, optical code-division-multiple-access, and optical packet generation. For example, RZ formats rather than non-return-to-zero (NRZ) formats have been applied in long-haul fiber transmission systems to extend transmission distance due to a possible higher tolerance to many fiber transmission impairments [38, 39]. As a result, the characteristics of RZ pulses in such systems play a critical role in optimizing system performance. Therefore, tunable RZ pulse generation is highly desirable in system contexts. Tunable width RZ pulses have been demonstrated based on various techniques [39–42]. The techniques in reference [39, 40] require electrical modulation which is difficult at high bit rates and/or shorter pulses. Optical tunable width RZ pulse generation has also been demonstrated [41, 42], but relies on a relatively complicated nonlinear optical processing scheme with higher optical power requirements and lower efficiency, and/or limited width/wavelength tunable range. Here, we demonstrate for the first time to our knowledge a linear optical technique for tunable RZ pulse generation and pulse width range ($\sim$ 3–50 ps) at 10 GHz repetition rate based on spectral line-by-line pulse shaping of a mode-locked laser. All-optical RZ-to-NRZ format conversion is also demonstrated using this method, which is desirable in optical networks where spectral efficiency is more important than transmission distance since the NRZ format is more spectrally efficient.

Fig. 12 shows the shaped spectra and corresponding waveforms, where the laser center wavelength is tuned to 1542 nm. The number of spectral lines is controlled by the slit width in the line-by-line pulse shaper. The waveforms in Fig. 12(a–d) are detected by a 50 GHz photo-diode and sampling scope after an optical amplifier. Fig. 12(a) shows 2 spectral lines separated by the 10 GHz laser repetition rate. The optical linewidths are limited by the 0.01 nm resolution of the optical spectrum analyzer used for this measurement. Other spectral lines are well blocked due to the high resolution line-by-line shaper. Since there are only two spectral lines, ideally the waveform intensity profile in the time domain corresponds to a cosine function (with a DC offset). The waveform in Fig. 12(a) indeed shows a cosine function with 50 ps width (FWHM). Fig. 12(b)-(d) show 3, 4 and 5 spectral lines transmitted through the line-by-line pulse shaper. Accordingly, the generated RZ pulses exhibit 33 ps, 25 ps and 20 ps widths respectively which clearly illustrate that tunable width optical RZ pulses have been produced. For generated pulses shorter than 20 ps, we measure them by standard short pulse intensity cross-correlation measurement, where an un-shaped 3 ps pulse is used as the reference. Fig. 12(e–g) show 6, 10, 16 and all spectral lines transmitted by the line-by-line pulse shaper, respectively. Accordingly, the generated RZ pulses are tuned from 16 ps to 3 ps (after de-convolution). The two pulses measured within each trace have different peak values due to non-perfect-alignment of the cross-correlation measurement apparatus. Fig. 12 demonstrates the width tunability of our method in a range of 3 ps to 50 ps. Assuming the optical bandwidth is (number of spectral lines -1) $\times$ 10 GHz, the time-bandwidth product of the generated pulses is in the range of 0.5–0.81 in Figs. 12(a)-(g). This is intermediate between that expected for transform limited sech pulses

(0.315) and for transform-limited pulses with rectangular spectrum (0.88). For the source limited 3 ps pulses, the 3 dB time-bandwidth product is approximately 0.33, close to transform limit for sech pulses.

We now use the line-by-line pulse shaping technique to achieve all-optical RZ-to-NRZ format conversion. Although the RZ format has been widely employed in long-haul fiber transmission systems as it has a higher tolerance for important impairments caused by fiber transmission effects, the NRZ format is more spectrally efficient and can be used in local and metro access networks where spectral efficiency is important. Therefore, all-optical RZ-to-NRZ format conversion is desirable at the interface between backbone and access networks. This conversion can be realized by various techniques, for example, based on relatively complicated nonlinear optical processing using SOA-based devices [43, 44], or cross-phase modulation in dispersion-shifted fiber [45]. Here we use line-by-line control, a linear technique, to achieve all-optical RZ-to-NRZ format conversion.

The generated RZ pulses are modulated and become an RZ format data stream. Fig. 13 (a) shows RZ format pulses modulated by a 10 Gb/s PRBS $2^{23} - 1$ data stream with 4 spectral lines (25 ps pulses) transmitted by the line-by-line pulse shaper. Compared with the un-modulated spectra shown in Fig. 12, each spectral line of the modulated spectra is broadened by the data modulation as shown in the figure. Here the line-by-line shaper is placed after the data modulator for experimental convenience. The modulated waveforms are detected by a 50 GHz photo-diode in which the RZ format is clear. In Fig. 13(b) only one spectral line is allowed to pass the line-by-line pulse shaper. As a result, the RZ format is converted to NRZ format, as shown by the eye-diagram also detected by the 50 GHz photo-diode. Higher spectral efficiency is clear for NRZ since it occupies less bandwidth with one spectral line rather than the bandwidth for RZ with multiple lines. The performance of the generated 25 ps RZ format and converted NRZ format are further confirmed by bit error rate measurement (not shown). For both formats, less than 10^{-10} bit error rate can be achieved using a standard 10 Gb/s receiver for both back-to-back and after 25 km single mode fiber transmission without dispersion compensation. In our experiment only a single line-by-line pulse shaper is used to emulate the RZ-to-NRZ format conversion. In practice, one line-by-line pulse shaper can be used to generate the RZ format with desired wavelength and width while utilizing another line-by-line pulse shaper to implement RZ-to-NRZ format conversion.

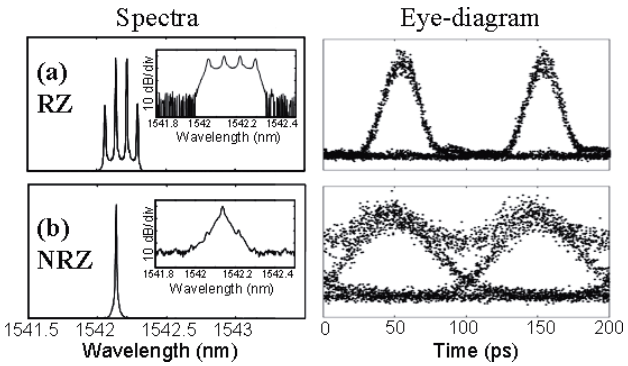

Figure 13 RZ-to-NRZ format conversion by line-by-line pulse shaping. Spectra and eye-diagrams for (a) data modulated RZ format with 4 spectral lines, (b) converted NRZ format with only one spectral line. Inset figures show the spectra in log scale.

In the current experiment the width of the RZ pulses is discretely tunable by simply changing the number of spectral lines. The pulse width can be continuously tuned by controlling not only the number of lines but also the relative amplitudes of the selected lines using a programmable amplitude line-by-line pulse shaper [8].

4. Impact of comb frequency instability on shaped waveforms

The waveforms generated via spectral line-by-line shaping are sensitive to the optical comb frequency instability. This sensitivity is fundamentally new in the line-by-line shaping regime and is not observed for group-of-line shaping. The impact of frequency comb instability on optical waveform generation can be apparent even for the simple case of selecting only two spectral lines with applied phase control [8]. The focus of this section is to model the impact of frequency comb stability on shaped waveforms [46]. A simple case employing only two spectral lines and independent phase control on these lines provides significant insight into the source of time-domain waveform instability. To provide a clear visualization, we compared the line-by-line phase control experiment and recorded both the optical spectra and sampling scope traces consecutively. With the actively mode-locked laser operating at 8.5 (relatively frequency stable) and at 10.5 (frequency unstable) GHz repetition rates, we can investigate the role of optical comb frequency fluctuations on line-by-line shaping.

Figs. 14(a,b) show an overlap of 100 scans for the two spectral lines and sampling scope traces for an 8.5 GHz pulse repetition rate, which show relatively stable features. If there is no pulse shaping ($\Phi = 0$), the sampling scope traces are clear, as shown in Fig. 14(b). If there is pulse shaping with $\Phi = \pi$ on one spectral line, the sampling scope traces become slightly noisy because of the small fluctuations of spectral lines. Nevertheless, the positions of the spectral lines are stable enough for line-by-line control, as demonstrated above.

When the laser repetition rate is tuned to 10.5 GHz, we observe empirically that the absolute frequency positions of the spectral lines become considerably less stable, with frequency fluctuations observable on a time scale of seconds, as shown in Fig. 14(c). We attribute the spectral line fluctuations in our actively mode-locked laser to comb-offset

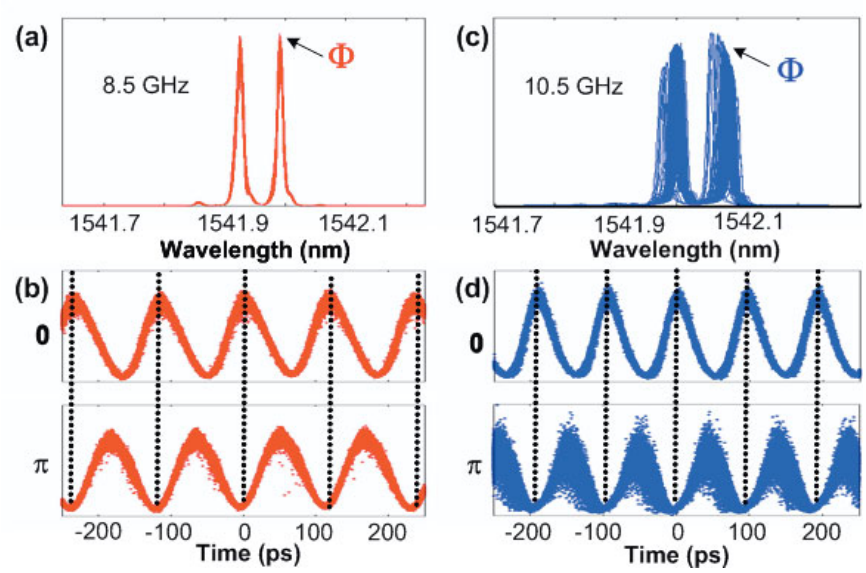

Figure 14 (online color at: www.lpr-journal.org) (a) Two relatively stable spectral lines at 8.5 GHz. (b) Sampling scope traces with phase modulation (0 and π) on one spectral line. The traces are scanned 100 times. (c) Two relatively unstable spectral lines at 10.5 GHz. (d) Sampling scope traces with phase modulation (0 and π) on one spectral line. The traces are scanned 100 times.

frequency fluctuations; we attribute the difference in optical frequency stability at different laser repetition rates to the frequency-dependent response of the microwave components used for feedback control of the cavity length. If there is no pulse shaping ($\Phi = 0$), under the conditions of our experiments the sampling scope traces are clear even if the spectral lines are relatively unstable, as shown in Fig. 14(d). However, if there is pulse shaping with a π phase shift on one spectral line, the sampling scope traces become extremely noisy because of the large fluctuations of the spectral line positions. This result can be understood from the time-domain overlap effect: For a π phase shift, the original laser pulses (corresponding to $\Phi = 0$) are reshaped to form waveforms with intensities in the temporal region where contributions from adjacent input pulses overlap. Since the adjacent original pulses have an unstable phase relationship (intimately related to unstable comb offset frequency), their interference in the overlapped region as a result of pulse shaping leads to large intensity fluctuations. Much weaker fluctuations, if any, are observed at the time locations of the original input pulses, as there is little temporal overlap at those times. Clearly, this overlap effect leads to observation of time-dependent noise that is directly linked to variations in the comb-offset frequency.

We hereby provide a frequency-domain analysis for clear elucidation of this issue [46]. Fig. 15 shows simulation results for the above two cases. Figs. 15(a, c) show the power spectrum of the comb (4 lines numbered from -2 to 2) with frequency offsets of -{0-50}% in 10% per increment with $\Phi = 0$ and π applied to line [-1], respectively. Lines [-1, 1] are selected. The effective shaper filter power spectra are denoted as the dashed traces. The initial frequency positions of the comb lines are marked by the arrows. The necessity of using 4 comb lines is to reflect the fact that although selecting only two central lines, lines [-2, 2] may participate in shaping for a large frequency offset, depending on the direction of the offset. The corresponding time-domain intensities are shown in Fig. 15(b, d) for $\Phi = 0$ and $\Phi = \pi$ cases, respectively.

In Fig. 15(a), for an initial zero frequency offset, only the central two lines pass through the filter, and result in a pure cosine time-domain intensity waveform. As the lines are frequency shifted together, line [-1] will be attenuated at the filter edge. The resulting time-domain intensity wave-

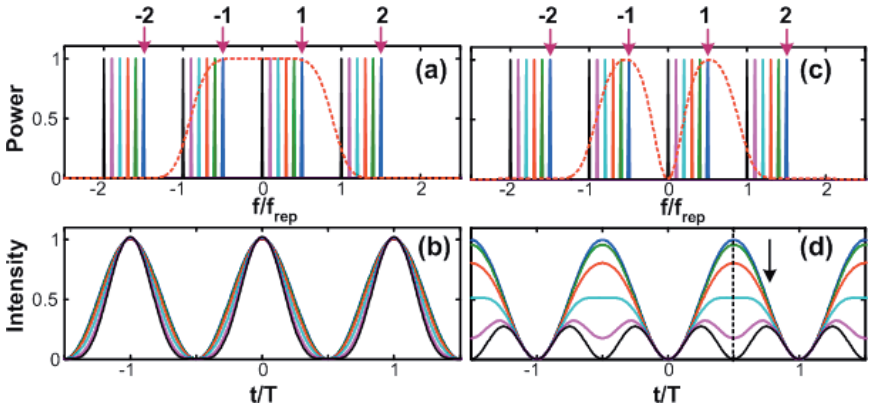

Figure 15 (online color at: www.lpr-journal.org) Frequency-domain simulations using 4 comb lines. Only lines $[-1, 1]$ are selected by the shaper filter. Normalized spectral powers with frequency offsets of {0–50}% with 10% per increment are shown for (a) $\Phi = 0$ and (c) $\Phi = \pi$. Resulting normalized time-domain intensities are shown in (b) $\Phi = 0$ and (d) $\Phi = \pi$.

form will have a slightly smaller peak. For large frequency offsets, line [2] enters the edge and participates in waveform generation, giving its contribution and compensating the spectral power and time-domain energy lost by line [-1]. As a consequence, the time-domain waveform suffers relatively small frequency-offset induced time-domain noise. Fig. 15(b) depicts a 10% intensity peak variation for a 50% frequency offset. The scenario is different for the $\Phi = \pi$ case, shown in Fig. 15(c) and 15(d). For the $\Phi = \pi$ case, note the filter function reveals an apparent spectral dip in the center, acts as a frequency discriminator, and is responsible for the higher time-domain noise. Both lines [-1, 1] are attenuated for having a frequency offset, due to the effective frequency discriminator, giving rise to a 68% intensity peak variation for 50% frequency offset. The arrow in Fig. 15(d) shows the evolution of the intensity waveform to larger offsets. Frequency-domain analysis is consistent with experimental observation and the discussions made for Fig. 14.

5. Shaping on alternative comb sources

5.1. Phase-modulated CW combs

Optical frequency combs are usually generated by mode-locked lasers emitting periodic trains of ultrashort pulses. Frequency-stabilized mode-locked lasers, such as self-referenced Ti:Sapphire lasers, are available at repetition rates (comb spacing) of ~ 5 GHz and below [47, 48]. Unfortunately current pulse shapers are unable to cleanly resolve such closely spaced spectral lines. Therefore, combs with larger line spacing are desired for line-by-line shaping; such combs also have the practical advantage of placing proportionally more power in individual lines. There are several alternative approaches for obtaining relatively frequency stable combs with higher repetition rate. Harmonically mode-locked lasers are well known but often exhibit optical frequency instabilities, which lead to serious pulse shape noise when employed for O-AWG. Examples of frequency-stabilized harmonically mode-locked lasers have been demonstrated, but only with complicated control and/or compromised frequency tunability [49, 50]. Approaches based on optical cavities are also relevant. For example, a Fabry-Perot cavity with free spectral range set to N times the comb spacing acts as a periodic transmission filter that passes only one of every N lines from an input comb source [4]. One may also generate a well-defined frequency comb by imposing a strong periodic phase modulation onto a continuous-wave (CW) laser, either without [51, 52] or with the aid of a cavity [53]. This PMCW scheme has the significant advantage that the frequency offset of individual lines is controlled by the input CW laser and decoupled from the pulse generation process. We adopt such a modulation-of-CW source with additional spectral broadening via nonlinear fiber optics as the input for our O-AWG demonstrations [54, 55].

Fig. 16(a) shows our experimental setup. A CW laser with specified 1 kHz linewidth centered at 1542 nm is modu-

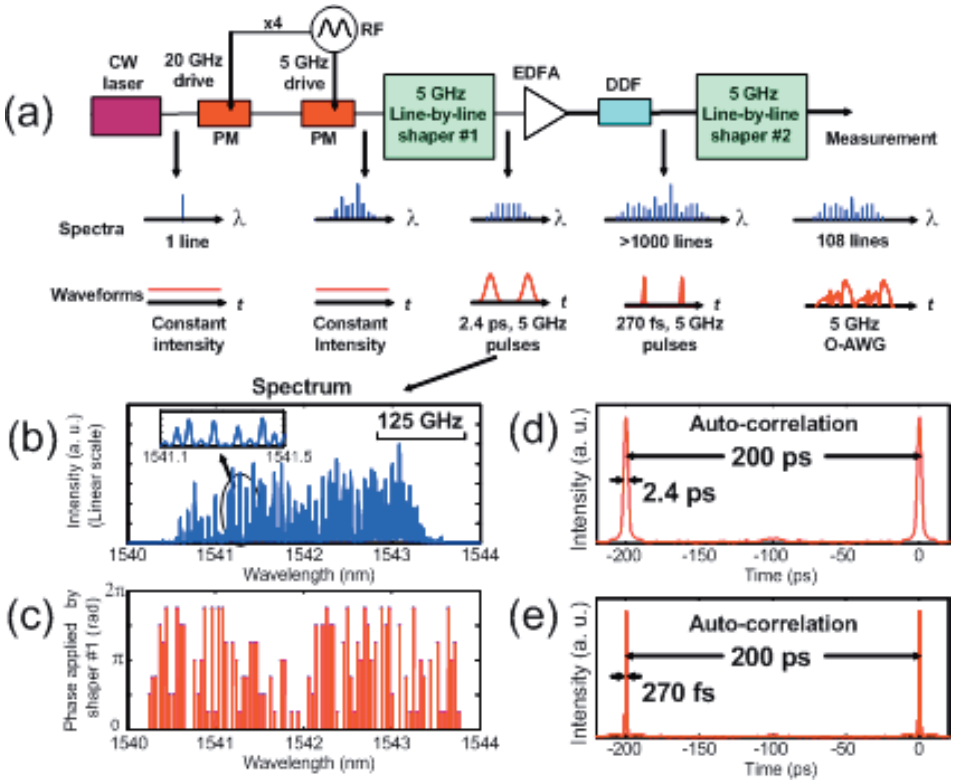

Figure 16 (online color at: www.lpr-journal.org) Experimental setup and high-rate ultrashort pulse generation. (a) Schematic diagram. (b) Spectrum (linear scale) after shaper #1. (c) Spectral phases applied by shaper #1. (d,e) Intensity auto-correlations after shaper #1 and DDF, respectively. PM: Phase modulator. RF: radio frequency. EDFA: Erbium doped fiber amplifier. DDF: Dispersion decreasing fiber.

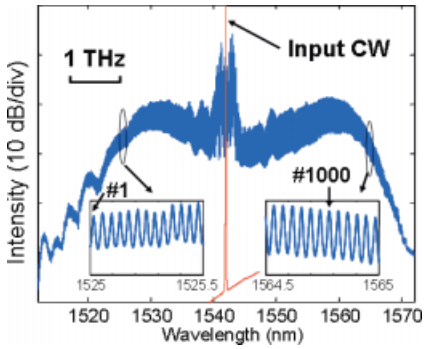

Figure 17 (online color at: www.lpr-journal.org) Generation of over 1000 stable spectral lines starting from 1 single line. Input CW is also shown for comparison.

lated by two phase modulators, driven synchronously (with adjustable delay) by 20 GHz and 5 GHz cosine waveforms. The phase modulator driven at 20 GHz contributes to broad bandwidth, since the generated bandwidth is proportional to the modulation frequency. The modulator driven at 5 GHz determines the comb spacing and temporal periodicity. The resulting comb is manipulated by spectral line-by-line pulse shaper #1 to convert the broadband constant intensity waveform to a pulse train. Here we use a line-by-line shaper with one LC pixel to control one comb line, separated by 5 GHz. Our experiments are the first to resolve comb lines spaced by only 5 GHz in a pulse shaping apparatus.

Fig. 16(b) shows the measured spectrum after shaper #1; the discrete lines making up the spectrum are clear in the inset. Fig. 16(c) shows the discrete spectral phases applied by shaper #1 onto the individual lines, in order to convert the phase-modulated but constant intensity field into bandwidth-limited 2.4 ps (FWHM) pulses (intensity autocorrelation shown in Fig. 16(d). Although not yet illustrating true O-AWG, such high rate pulse generation starting from a CW source is already a powerful application of line-by-line pulse shaping [56]. The 2.4 ps pulses are then amplified by a fiber amplifier and directed into a dispersion decreasing fiber (DDF) soliton compressor. The interplay of self-phase modulation and dispersion in the DDF yield pulse compression to durations as short as 270 fs (Fig. 16(e)). Pulse compression is accompanied by strong spectral broadening. Fig. 17 shows the spectrum after DDF compression obtained with slightly higher optical power coupled into the DDF. Over 1000 lines are generated between 1525 nm and 1565 nm.

Such a comb, created from a single CW laser, is highly useful for line-by-line pulse shaping studies. In our following O-AWG demonstrations we use a second line-by-line pulse shaper following the DDF (see Fig. 16(a)) to select and individually manipulate a set of 108 lines centered around 1537.5 nm and spanning 540 GHz bandwidth. The spectrum is shown in Fig. 18(a). An intensity cross-correlation measurement of the resulting pulse train, demonstrating transform-limited 1.65 ps pulses at 5 GHz repetition rate, is also shown. In this and subsequent measurements, temporal intensity waveforms are obtained via cross-correlation with high quality, pedestal-free, 1.02 ps reference pulses. The reference pulses are obtained by sending a portion of the output power after the DDF to another high resolution pulse shaper, where only the spectrally smooth portion is selected. Fig. 18(b) demonstrates a simple example of line-by-line intensity control, where the LCM is programmed to block every other comb line. The resultant doubling of the comb spacing leads in the time domain to a doubling of the pulse repetition rate to 10 GHz.

We demonstrate the capability of line-by-line phase control for O-AWG by exploiting the relation $\tau(\omega) = -\frac{\partial \Psi(\omega)}{\partial \omega}$, where $\tau(\omega)$ and $\Psi(\omega)$ are the frequency-dependent delay and spectral phase, respectively. In the simplest case we apply linear spectral phase, which results in pure delay as shown in Fig. 19. Notice that the delay is scanned across the whole repetition period T (200 ps), which is only possible when individual spectral comb lines are independently manipulated. The waveforms remain clean, with only very small satellite pulses. This is further evidence that we are in the line-by-line regime. In the group-of-lines regime, a strongly stepped masking function gives rise to significant satellite pulses, with satellite intensity becoming equal to main pulse intensity at phase steps of π per pixel [57].

Fig. 20 shows examples of O-AWG with highly structured temporal features: each pulse is split into two pulses per period, one of which is delayed and the other of which

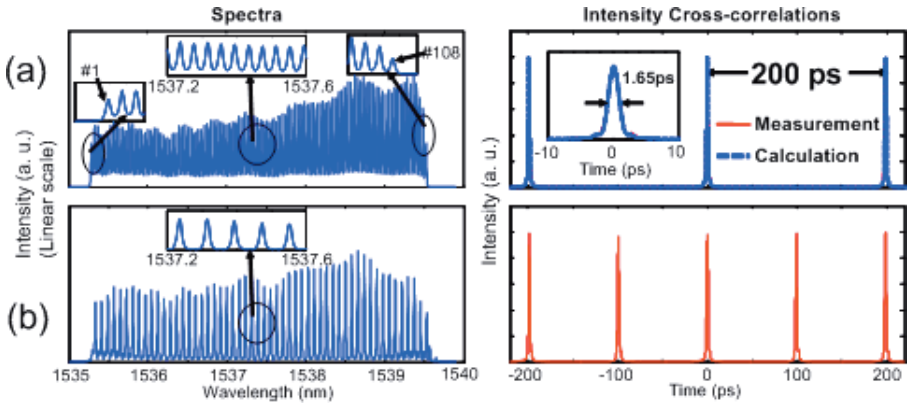

Figure 18 (online color at: www.lpr-journal.org) Line-by-line intensity control of 108 lines. (a) Spectrum and intensity cross-correlation. Calculated intensity cross-correlation is also shown for comparison. (b) Spectrum and intensity cross-correlation by blocking every other line.

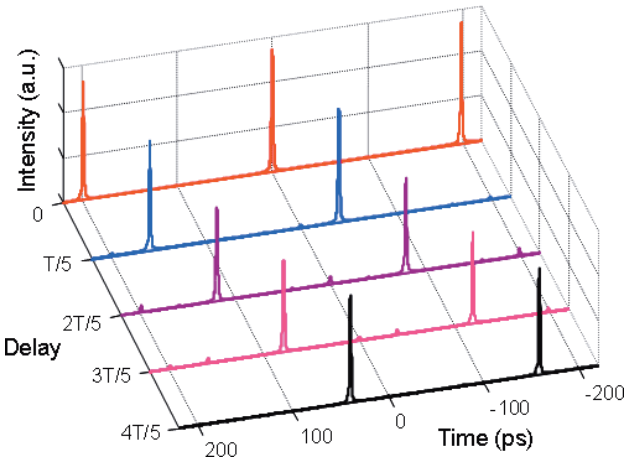

Figure 19 (online color at: www.lpr-journal.org) Line-by-line phase control of 108 lines: In a series of experiments, the pulse shaper applies various linear spectral phase ramps, resulting in delays proportional to the slope of the applied phase ramp. Intensity cross-correlation measurements are plotted for pulse trains delayed by 0, T/5, 2T/5, 3T/5 and 4T/5, respectively.

has cubic spectral phase. In contrast to the data of section (3.3), here we chose to program the shaper such that the delayed pulse and the cubic spectral phase pulse correspond to different halves of the spectrum. Fig. 20(a) shows an example. The cubic spectral phase corresponding to quadratic frequency-dependent delay yields a strongly oscillatory tail in the time domain that spans the whole period with 100% duty cycle, which is one of the hallmarks of line-by-line pulse shaping. To confirm O-AWG fidelity, the calculated intensity cross-correlations are also shown for comparison. The agreement is excellent everywhere, even in the lowest intensity oscillations. Figs. 20(b, c) show the unwrapped and wrapped discrete spectral phases applied to the 108 lines by shaper #2. The linear and cubic spectral phases are clearly visible on respective halves of the spectrum. At some locations the phase change per pixel is π or more – again a hallmark of operation in the line-by-line regime.

One important aspect of this setup is that it is scalable in both spectral line generation and spectral line manipulation. Our comb generator already provides >1000 frequency stable spectral lines available for future O-AWG investigations, and further nonlinear spectral broadening should be possible. By developing pulse shapers based on novel two-dimensional spectral dispersers [58], a radically increased number of control elements should be possible, considering the large array technologies in use for two-dimensional display applications.

5.2. Optical frequency comb generator (OFCG)

An elegant extension of the phase modulated CW scheme to generate an ultra broadband comb (Terahertz and more) has been proposed and demonstrated a number of years ago [53, 59–66]. This device, called an optical frequency comb generator (OFCG), is an electro-optic ($LiNbO_3$) modulator inside a Fabry-Perot cavity (the cavity can also be formed by coating high reflectors on the facets of the $LiNbO_3$ crystal/waveguide), schematically shown in Fig. 21(a). With this resonant configuration, the OFCG is able to generate a very wide optical frequency comb (up to tens of THz) [53, 59]. The cavity configuration of the OFCG, similar to a laser cavity, provides feedback and a resonance mechanism so that the efficiency of the modulation is increased significantly by multiple passes of light

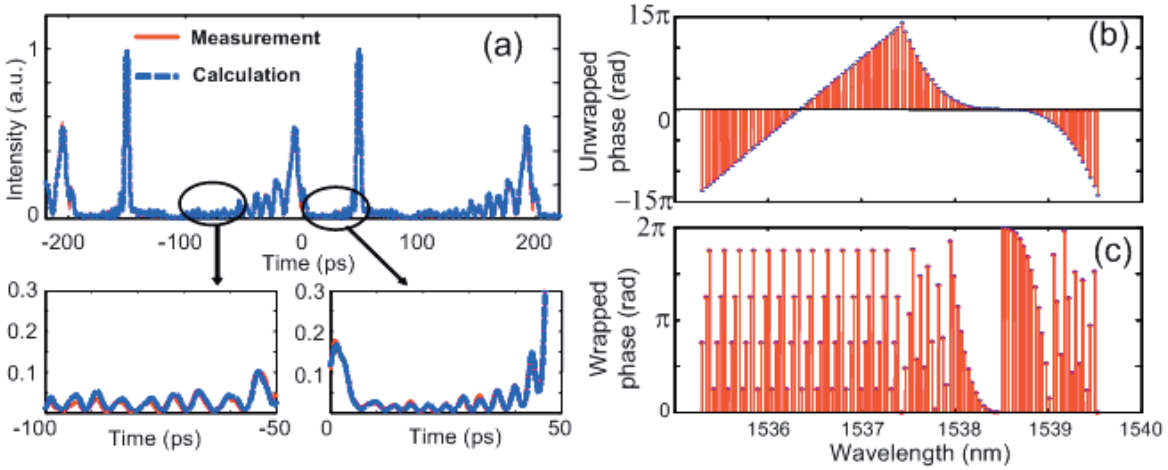

Figure 20 (online color at: www.lpr-journal.org) Line-by-line shaping of 108 lines: O-AWG with high temporal complexity. (a) The intensity cross-correlation: each pulse is split into two pulses per period, one of which is delayed and the other of which has cubic spectral phase. Each pulse corresponds to one half of the spectrum. The two pulses are still temporally separated. Solid line: measured intensity cross-correlation. Dashed line: calculated intensity cross-correlation. (b) The unwrapped spectral phases applied to shaper #2. (c) The wrapped spectral phases applied to shaper #2.

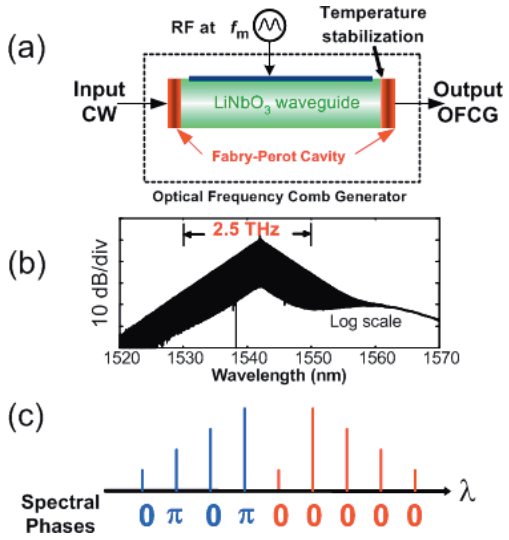

Figure 21 (online color at: www.lpr-journal.org) (a) Schematic diagram for the optical frequency comb generator (OFCG). (b) Experimental OFCG output spectrum. (c) Schematic of the spectral phases for intrinsic dual-pulsed generation from an OFCG.

through the modulator, giving broader bandwidth than both phase modulated CW lasers and mode-locked lasers at ~ 10 GHz line spacing. Since the OFCG has both characteristics of a phase modulated CW and a mode-locked laser, it is expected to combine their advantages. The OFCG's similarity to a phase modulated CW makes it easy to tune the comb offset frequency by simply changing the input CW wavelength and the spectral line position is stable, which is critical for line-by-line pulse shaping. The OFCG's similarity to a mode-locked laser makes it have a smooth spectrum without dips, as shown in Fig. 21(b).

In the time domain, a comb with broad bandwidth from the OFCG supports periodic short pulses similar to mode-locked lasers. However, distinct from mode-locked lasers, the intensity repetition rate is twice the comb spacing (i.e., there are 2 pulses in each period). Pulses from the OFCG and their characteristics have also been investigated, but exclusively concentrating on the pulses directly from the OFCG [64–66]. Roughly speaking, the 2 pulses in each period correspond to the lower and upper half of the spectrum of the frequency comb, respectively. Illustrated in Fig. 21(c), starting from the center line, all spectral lines from one half spectrum have zero spectral phases while the spectral lines from the other half spectrum have alternative 0 and π spectral phases. Therefore, the overall waveform is not transform limited and the individual pulse widths are determined by the bandwidth of one-half of the spectrum.

The cavity used in our experiments has a 2.50 GHz free spectral range (FSR) with cavity length temperature stabilized [67]. The finesse of the cavity is 55. RF driving frequencies with an integer number times the FSR are required to meet the resonance conditions as 10.00 GHz is used in our experiments. The OFCG has ~ 28 dB loss. To compensate this relatively large loss, we used 60 mW input CW power and use an EDFA after the comb generator as well. The output power of the EDFA after the OFCG is around 20 mW.

The OFCG is capable of generating a large number of lines. However, the number of lines to be shaped in our setup is currently limited by the available 128 pixels of the LCM. Since 2 pixels control one line, 64 lines in total can be used for line-by-line pulse shaping demonstrations. We expect this can be extended to hundreds of lines with a commercially available 640-pixel LCM.

Fig. 22(a) shows the 64 lines after quadratic phase correction for dispersion compensation by spectral line-by-line pulse shaping. The applied quadratic phase shift corresponds to opposite dispersion from 45.4 m of single mode fiber (SMF), which is consistent with the fiber links used in our system. Consequently, the resultant pulses are similar to those directly from the OFCG (with a bandwidth of 64 lines) without fiber dispersion distortions. Intensity cross-correlation shows two single peak pulses in each period as expected. For our cross-correlation measurements, a portion of the OFCG output power is sent to another high resolution shaper. The shorter wavelength half of the OFCG comb was selected to provide the 1.20 ps reference pulses.

Fig. 22(b) and 22(c) show pulse measurement for each half of the spectrum. The pulse shaper is programmed to block either half spectrum in addition to adding a quadratic phase (the center line is assigned to the long wavelength half spectrum) for dispersion compensation. As expected, each trace corresponds to a clean pulse train at 10 GHz with a relative 50 ps delay. Also note that auto-correlation cannot give correct delay information while cross-correlation and sampling scope traces can.

Fig. 22(d) shows the capability of combining two pulses in each period into one single transform limited pulse. The 64 lines have been used for line-by-line pulse shaping to achieve shorter pulses than that from each half spectrum. We apply alternative 0 and π phase shift on the short wavelength half of the spectrum (32 lines) to correct the spectral phases caused by the OFCG itself; we also overlay the quadratic phase shift for fiber dispersion compensation. As a result, two pulses in each period have been successfully combined to one single nearly transform limited pulse as shown by auto-correlation, cross-correlation and sampling scope traces. Here we move the pulse at 50 ps delay to the 0 ps position. By applying a different phase, we can also move the pulse at 0 ps to the 50 ps position. Since the combined pulse corresponds to the whole spectrum, it should have shorter pulse width compared with individual pulses from each half of the spectrum (roughly speaking the pulse width is reduced by two). For each filtered half spectrum, the pulses are 2.83 ps (b) and 2.88 ps (c), respectively. The slight difference between each half of the full spectrum is caused by a different spectral profile for each half of the spectrum. After line-by-line pulse shaping to combine two pulses into one single pulse, the pulse for the whole 64 lines becomes shorter as expected. Fig. 22(e) shows a shorter temporal scale where the resemblance is

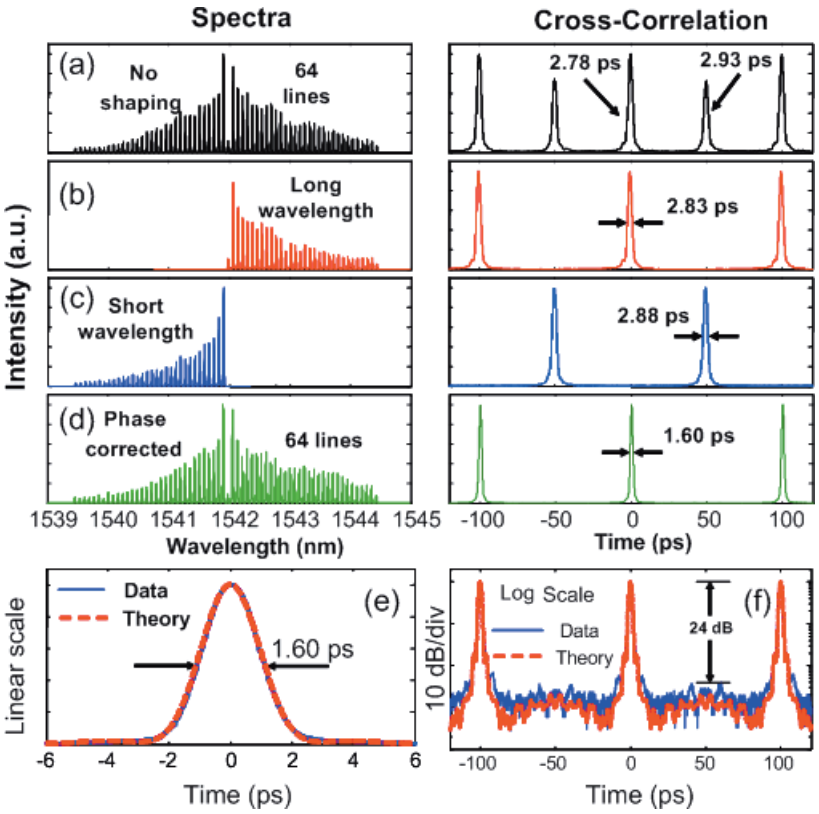

Figure 22 (online color at: www.lpr-journal.org) Spectra and intensity cross-correlations. (a) 64 lines with dispersion compensation. (b) long wavelength half 32 lines with dispersion compensation. (c) short wavelength half 32 lines with dispersion compensation. (d) 64 lines after full phase correction. Two pulses in each period are combined to one single transform limited pulse. (e) Magnified view on the combined pulse in linear scale. (f) Combined pulse in log scale.

clear. Both auto-correlations give 2.20 ps FWHM without de-convolution. The calculated transform limited pulse has 1.60 ps FWHM. These results suggest that we generated 10 GHz repetition rate, 1.60 ps essentially transform limited pulses by line-by-line pulse shaping of 64 lines. Fig. 22(f) shows auto-correlations in log scale, which again shows the close resemblance between measured and calculated traces even in the wings. The pulse train has high quality without satellite pulses and pedestal suppression of greater than 24 dB in the measured auto-correlation.

6. 10-GHz programmable microwave waveform generation

In our previous sections, we have demonstrated shaping examples where the waveform update rate is limited by the response time of the LCM, typically tens of milliseconds. Recently, there have been several reported efforts to increase the waveform update rate, with results demonstrated up to 33 MHz [68–70]. However, due to limited spectral resolution, groups rather than individual spectral lines have been manipulated in these works.

A hyperfine wavelength de-multiplexer with subsequent electro-optical modulators have been reported with a waveform modulation rate ranging from tens to hundreds of MHz, but only two spectral lines were controlled [9, 71, 72]. In a previous demonstration, our group reported switching between two optical waveforms at 10 GHz in the group-of-lines shaping regime; however, each waveform required a separate shaper [73]. Here we report a novel scheme where distinct waveforms can be generated at high update speed using a single pulse shaper.

Photonically assisted radio frequency arbitrary waveform generation (RF-AWG) [74] is a promising application of pulse shaping that has been demonstrated previously at low pulse shaping resolution and with low update rate [75, 76]. In this part, we overcome the limitation of the LCM response time and report a simple structure which allows RF-AWG waveform updates in less than 100 ps (10 GHz), to our knowledge the fastest reported to date [77].

The schematic of our proposed novel time-multiplexed setup is shown in Fig. 23. Two CW lasers (λ_a, λ_b) with a $LiNbO_3$ intensity modulator (IM) after each laser are used to provide rapid wavelength switching. IM1 (for λ_a) and IM2 (for λ_b) are driven by the programmable data port (Q) and inverted data port ($\bar{Q}$) of a bit-error-ratio test set (BERT) with bit duration of 100 ps (10 GHz signal), respectively. The wavelength switched CW outputs are combined via an optical coupler (node (i)) and sent to an optical frequency comb generator comprised of a lithium niobate phase modulator (PM) driven at a repetition frequency of $f_{\text{rep}} = 10$ GHz by the clock of the BERT (node (ii)). These phase-modulated CW (PMCW) combs are manipulated by a line-by-line shaper where distinct waveforms are generated for each different input center wavelengths (node (iii), $I_a(t)$ and $I_b(t)$).

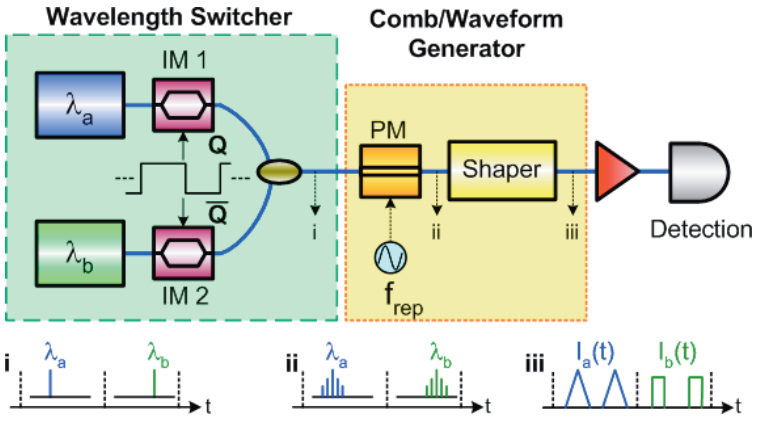

Figure 23 (online color at: www.lpr-journal.org) Schematic of the experimental setup. (λ_a, λ_b): two CW lasers; IM: intensity modulator; Q: data pattern; PM: phase modulator; f_{rep}: comb frequency spacing.

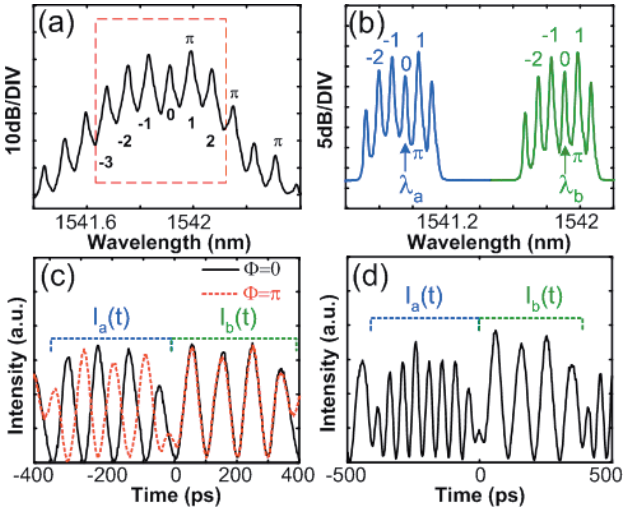

Figure 24 (online color at: www.lpr-journal.org) (a) PMCW spectrum. Six lines within the rectangle are used for waveform generation. (b) Six-line selected PMCW combs when both CW lasers are on. (c, d) Sampling scope traces of rapid RF-AWG updates with Q=[1111 0000]. (c) Switching between waveform phase modulation using two spectral lines from each comb. (d) Switching between waveform frequencies.

In order to enable high-speed waveform updates, the LCM pixels are logically divided into different regions, each of which may be programmed to generate different waveforms; each region may be selected by rapidly changing the input wavelength. An optical amplifier is used after the shaper and the rapid-updated waveforms are detected using a 50 GHz bandwidth sampling scope/photodiode. An optical spectrum analyzer (OSA) with 0.01 nm resolution is used to measure the comb spectra.

In order to more clearly explain the concept, first consider the use of only one CW laser. Fig. 24(a) shows the λ_b PMCW comb (line $\{0\}$ denotes the CW input). The spectral lines that have a π-phase difference are labeled within the figure. Note that without phase correction, the time-domain output intensity of the PMCW comb is still CW in nature. In our experiments, lines $\{-3 \sim 2\}$ are selected by the line-by-line shaper to demonstrate shaped waveform updates so that the optical bandwidth does not exceed the electrical bandwidth of our sampling scope. Fig. 24(b) shows the six-line PMCW combs when both CW lasers are turned on with $\lambda_a = 1540.95$ nm and $\lambda_b = 1541.91$ nm. As a first demonstration of shaped RF-AWG updates, Fig. 24(c) shows rapid waveform switching, in which a repetitive data pattern $Q = [1111\ 0000]$ is fed to IM1. Here, two cosine waveforms (spectral lines $\{a_{-1}, a_0\}$ and $\{b_{-1}, b_0\}$ selected while others are suppressed) are generated. The corresponding intensity waveforms $I_a(t)$ and $I_b(t)$ are labeled within the figure. The solid trace indicates the measured waveform when no optical phase control is applied, and I_a and I_b are identical cosine waveforms. Switching between I_a and I_b simply results in a continuous RF cosine signal shown in the figure (although transient effects are evident with a reduction in signal amplitude near the wavelength switching times). The dashed trace indicates the measured waveform when a π phase is applied to line $\{a_{-1}\}$ so that I_a is delayed by exactly half the period compared to I_b. This yields an RF waveform with abrupt π phase shifts inserted at times determined by the driving data. Fig. 24(d) shows rapid switching of waveform frequencies. Here lines $\{a_{-1}, a_1\}$ are selected for the λ_a comb, resulting in a cosine waveform with repetition rate of $2f_{\text{rep}}$, while the λ_b comb is again filtered to yield a cosine waveform with repetition rate of f_{rep}. Rapid switching between the two waveforms is observed in direct correspondence to the data pattern. The update transition time is less than 100 ps, defined here by the data pattern frequency (10 GHz).

Fig. 25 demonstrates signals incorporating rapid triangular waveforms. These are obtained by applying a cubic spectral phase to a broader PMCW comb (using dual stage phase-modulation) resulting in oscillatory tails, so that a triangular RF waveform is converted via the photo-detector. The resulting PMCW spectra are shown in Fig. 25(a), where 28 spectral lines (280 GHz bandwidth) are selected from each comb. The spectral line phases are corrected using an automated process, resulting in transform-limited pulses. On top of these phase corrections, a cubic spectral phase is applied to the λ_a comb, resulting in rapid updates between triangular and transform-limited pulses, shown in

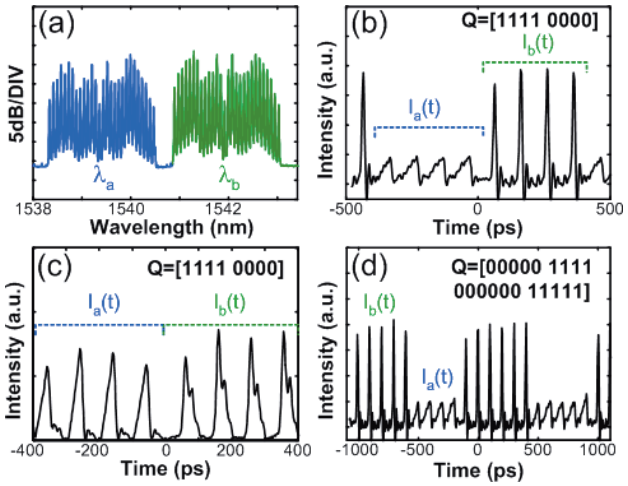

Figure 25 (online color at: www.lpr-journal.org) (a) 28-line PMCW combs used for triangular RF waveforms. (b) Switching between triangular and transform-limited pulses. (c) Switching between triangular waves with opposite (fast, slow) trailing edges. (d) Waveform switching using a more complicated data pattern.

Fig. 25(b). Fig. 25(c) shows the waveforms when the λ_b comb has an applied cubic phase of opposite sign to that of the λ_a comb, providing triangular pulse updates with opposite {fast, slow} edges. The slight ripples observed on the trailing edge of $I_b(t)$ are due to the detector impulse response. In these two examples, $Q = [1111\ 0000]$ is used. To demonstrate flexibility of data patterning, Fig. 25(d) shows waveform updates using a repetitive 20-bit-length data pattern.

In summary, using a simple configuration, we demonstrate, to the best of our knowledge, the fastest time-multiplexed RF arbitrary waveform generation ever reported. By combining 10-GHz wavelength switching, optical comb generation, and liquid crystal modulator based line-by-line pulse shaping, RF-waveforms are updated within 100 ps.

7. Conclusion

In conclusion, we have demonstrated the capability of high-fidelity O-AWG with 100% duty factor using spectral line-by-line pulse shaping. Line-by-line shaping on harmonically mode-locked fiber laser combs, PMCW combs, and OFCG are shown. O-AWG examples of simple repetition-rate multiplication, optical arbitrary pulse train generation, radio-frequency waveform generation, and very complicated waveforms using more than 100 spectral lines are experimentally performed. The capability to rapidly switch between desired microwave waveforms with 10 GHz rate is also demonstrated. Combining the detailed spectral control available from pulse shaping with the high coherence of short pulse frequency comb sources ushers in a new level of control over pulsed optical fields.

Chen-Bin Huang received the B. S. degree in electrical engineering from National Tsing Hua University, Hsinchu, Taiwan in 1997, the M. S. degree in electro-optical engineering from National Chiao Tung University, Hsinchu, Taiwan in 1999 and the Ph. D. from the School of Electrical and Computer Engineering, Purdue University, West Lafayette, IN, USA in 2008.

His current research interests include optical and RF arbitrary waveform generations and characterizations of optical frequency combs. From 1999 to 2003, he joined the Opto-Electronics & Systems Laboratories (OES), Industrial Technology Research Institute (ITRI), Taiwan as research engineer, developing passive fiber optical and photonic crystal devices.

Mr. Huang was awarded with the Master's Thesis of the Year by the Optical Engineering Society of Republic of China in 1999, Personal Research Achievement Award by OES, and Personal Distinguished Research Achievement Award by ITRI, both in 2002. He received the Andrews and Mary I. Williams Fellowship at Purdue University, in 2004 and 2005. He was selected as a finalist for the LEOS 2007 Best Student Paper Award.

Zhi Jiang received the B. S. (highest honors) and M. S. degrees in electronics engineering from Tsinghua University, Beijing, China, in 1999 and 2002, respectively, and the Ph. D. degree in electrical and computer engineering from Purdue University, West Lafayette, IN, in 2006.

He is currently a Beckman Institute Postdoctoral Fellow, University of Illinois at Urbana-Champaign (UIUC). His research interests include biomedical optics, ultrafast optics and fiber optics.

During his Ph. D. study, Dr. Jiang received the Ross and Mary I. Williams Fellowship from Purdue University and the 2005 IEEE/LEOS Graduate Student Fellowship. He was selected as a finalist for the 2005 OSA New Focus/Bookham Student Award and a finalist for the Purdue-Chorafas Best Thesis Award for his Ph. D. thesis work. He was a recipient of the 2005 Chinese Government Award for Outstanding Graduate Students Abroad. In 2007, he was selected as one of the four recipients of the Beckman Postdoctoral Fellowship.

Daniel E. Leaird received the B. S. degree in physics from Ball State University, Muncie, IN, in 1987, and the M. S. and Ph. D. degrees from the School of Electrical and Computer Engineering, Purdue University, West Lafayette, IN, in 1996 and 2000, respectively.

He joined Bell Communications Research (Bellcore), Red Bank, NJ, as a Senior Staff Technologist in 1987, and later advanced to Member of Technical Staff. From 1987 to 1994, he worked in the Ultrafast Optics and Optical Signal Processing Research Group, where he was a key team member in research projects in ultrafast optics, such as shaping of short optical pulses using liquid crystal modulator arrays, investigation of dark soliton propagation in optical fibers, impulsive stimulated Raman scattering in molecular crystals, and all-optical switching.

Dr. Leaird is currently a Senior Research Scientist and Laboratory Manager of the Ultrafast Optics and Optical Fiber Communications Laboratory in the School of Electrical and Computer Engineering, Purdue University. He has co-authored approximately 80 journal articles, 100 conference proceedings, and has three issued U. S. patents.

Dr. Leaird has received several awards for his work in the ultrafast optics field including a Bellcore "Award of Excellence", a Magoon Award for outstanding teaching, and an Optical Society of America/New Focus Student Award.

José Caraquitena received the B. S., M. S., and Ph. D. degrees in physics from the Universidad de Valencia, Valencia, Spain, in 1999, 2001, and 2004, respectively. His thesis work was focused on space–time dualities and propagation of ultrashort pulsed-beams in free-space dispersion-compensated optical setups.

From May 2005 to mid-2007, he was a Postdoctoral Research Fellow with the Ultrafast Optics and Optical Fiber Communications Laboratory, School of Electrical and Computer Engineering, Purdue University, West Lafayette, IN, where he performed research on spectral line-by-line pulse shaping. Since July 2007, he is a Research Associate in the Nanophotonics Technology Center, Universidad Politécnica de Valencia, Valencia, Spain. His current research interests include optical signal processing and microwave photonics.

Andrew M. Weiner graduated from M. I. T. in 1984 with an Sc. D. in electrical engineering. Upon graduation he joined Bellcore, first as Member of Technical Staff and later as Manager of Ultrafast Optics and Optical Signal Processing Research. Prof. Weiner moved to Purdue University in 1992 and is currently the Scifres Distinguished Professor of Electrical and Computer Engineering. His research focuses on ultrafast optics signal processing and applications to high-speed optical communications and ultrawideband wireless. He is especially well known for his pioneering work in the field of femtosecond pulse shaping. He is a Fellow both of the Optical Society of America and of the Institute of Electrical and Electronics Engineers (IEEE) and a member of the National Academy of Engineering. He has won numerous awards for his research, including the Hertz Foundation Doctoral Thesis Prize (1984), the Adolph Lomb Medal of the Optical Society of America (1990), the Curtis McGraw Research Award of the American Society of Engineering Education (1997), the International Commission on Optics Prize (1997), the IEEE LEOS William Streifer Scientific Achievement Award (1999), the Alexander von Humboldt Foundation Research Award for Senior U. S. Scientists (2000), and the inaugural Research Excellence Award from the Schools of Engineering at Purdue (2003).

Prof. Weiner has published six book chapters and over 200 journal articles and has been author or co-author of over 350 conference papers. He is holder of 10 U. S. patents. Prof. Weiner has served as Co-Chair of the Conference on Lasers and Electro-optics and the International Conference on Ultrafast Phenomena. He has also served as Secretary/Treasurer of IEEE LEOS and as a Vice-President of the International Commission on Optics (ICO).

References

[1] A. M. Weiner, Femtosecond pulse shaping using spatial light modulators, Rev. Sci. Instrum. **71**, 1929–1960 (2000).
[2] T. Udem, R. Holzwarth, and T. W. Hansch, Optical frequency metrology, Nature **416**, 233–237 (2002).
[3] A. Marian, M. C. Stowe, J. R. Lawall, D. Felinto, and J. Ye, United time-frequency spectroscopy for dynamics and global structure, Science **306**, 2063–2068 (2004).
[4] S. A. Diddams, L. Hollberg, and V. Mbele, Molecular fingerprinting with the resolved modes of a femtosecond laser frequency comb, Nature **445**, 627–630 (2007).
[5] M. J. Thorpe, K. D. Moll, R. J. Jones, B. Safdi, and J. Ye, Broadband cavity ringdown spectroscopy for sensitive and rapid molecular detection, Science **311,** 1595–1599 (2006).
[6] J. Capmany and D. Novak, Microwave photonics combines two worlds, Nature Photonics **1**, 319–330 (2007).
[7] W. C. Swann and N. R. Newbury, Frequency-resolved coherent lidar using a femtosecond fiber laser, Opt. Lett. **31**, 826–828 (2006).
[8] Z. Jiang, D. S. Seo, D. E. Leaird, and A. M. Weiner, Spectral line-by-line pulse shaping, Opt. Lett. **30**, 1557–1559 (2005).
[9] T. Yilmaz, C. M. DePriest, T. Turpin, J. H. Abeles, and P. J. Delfyett, Toward a photonic arbitrary waveform generator using a modelocked external cavity semiconductor laser, IEEE Photonics Technol. Lett. **14**, 1608–1610 (2002).
[10] Z. Jiang, D. E. Leaird, and A. M. Weiner, Line-by-line pulse shaping control for optical arbitrary waveform generation, Opt. Express **13**, 10431–10439 (2005).
[11] M. M. Wefers and K. A. Nelson, Generation of high-fidelity programmable ultrafast optical waveforms, Opt. Lett. **20**, 1047–1049 (1995).

[12] J. D. McKinney, D. E. Leaird, and A. M. Weiner, Millimeter-wave arbitrary waveform generation with a direct space-to-time pulse shaper, Opt. Lett. **27**, 1345–1347 (2002).
[13] M. Z. Win and R. A. Scholtz, Ultra-wide bandwidth time-hopping spread-spectrum impulse radio for wireless multiple-access communications, IEEE Trans. Commun. **48**, 679–691 (2000).
[14] E. Rothwell, D. P. Nyquist, K. M. Chen, and B. Drachman, Radar target discrimination using the extinction-pulse technique, IEEE Trans. Antennas Propag. **AP-33**, 929–937 (1985).
[15] T. Sizer, II, Increase in laser repetition rate by spectral selection, IEEE J. Quantum Electron. **25**, 97–103 (1989).
[16] P. Petropoulos, M. Ibsen, M. N. Zervas, and D. J. Richardson, Generation of a 40-GHz pulse stream by pulse multiplication with a sampled fiber Bragg grating, Opt. Lett. **25**, 521–523 (2000).
[17] K. Yiannopoulos, K. Vyrsokinos, E. Kehayas, N. Pleros, K. Vlachos, H. Avramopoulos, and G. Guekos, "Rate multiplication by double-passing Fabry–Pérot filtering," IEEE Photonics Technol. Lett. **15**, 1294–1296 (2003).
[18] S. Arahira, S. Kutsuzawa, Y. Matsui, D. Kunimatsu, and Y. Ogawa, Repetition frequency multiplication of mode-locked pulses using fiber dispersion, J. Lightwave Technol. **16**, 405–410 (1998).
[19] I. Shake, H. Takara, S. Kawanishi, and M. Saruwatari, High-repetition-rate optical pulse generation by using chirped optical pulses, Electron. Lett. **34**, 792–793 (1998).
[20] S. Longhi, M. Marano, P. Laporta, O. Svelto, M. Belmonte, B. Agogliati, L. Arcangeli, V. Pruneri, M. N. Zervas, and M. Ibsen, 40-GHz pulse-train generation at 1.5 µm with a chirped fiber grating as a frequency multiplier, Opt. Lett. **25**, 1481–1483 (2000).
[21] J. Azaña and M. A. Muriel, Temporal self-imaging effects: theory and application for multiplying pulse repetition rates, IEEE J. Sel. Top. Quantum Electron. **7**, 728–744 (2001).
[22] J. Caraquitena, Z. Jiang, D. E. Leaird, and A. M. Weiner, Tunable pulse repetition-rate multiplication using phase-only line-by-line pulse shaping, Opt. Lett. **32**, 716–718 (2007).
[23] M. R. Schroeder, Number Theory in Science and Communication (Springer-Verlag, Berlin, Heidelberg, 1986), pp. 180.
[24] C.-B. Huang and Y. C. Lai, Loss-less pulse intensity repetition-rate multiplication using optical all-pass filtering, IEEE Photonics Technol. Lett. **12**, 167–169 (2000).
[25] C. J. S. de Matos and J. R. Taylor, Tunable repetition-rate multiplication of a 10 GHz pulse train using linear and nonlinear fiber propagation, Appl. Phys. Lett. **83,** 5356–5358 (2003).
[26] D. Pudo and L. R. Chen, Tunable passive all-optical pulse repetition rate multiplier using fiber Bragg gratings, J. Lightwave Technol. **23**, 1729–1733 (2005).
[27] J. A. Bolger, P. F. Hu, J. T. Mok, J. L. Blows, and B. J. Eggleton, Talbot self-imaging and cross-phase modulation for generation of tunable high repetition rate pulse trains, Opt. Commun. **249**, 431–439 (2005).
[28] J. D. McKinney, D. S. Seo, D. E. Leaird, and A. M. Weiner, Photonically assisted generation of arbitrary millimeter-wave and microwave electromagnetic waveforms via direct space-to-time optical pulse shaping, J. Lightwave Technol. **21**, 3020–3028 (2003).
[29] B. Xia and L. R. Chen, Ring resonator arrays for pulse repetition rate multiplication and shaping, IEEE Photonics Technol. Lett. **18**, 1999–2001 (2006).
[30] B. Xia, L. R. Chen, P. Dumais, and C. L. Callender, Ultrafast pulse train generation with binary code patterns using planar lightwave circuits, Electron. Lett. **42**, 1119–1120 (2006).
[31] Z. Jiang, C.-B. Huang, D. E. Leaird, and A. M. Weiner, Spectral line-by-line pulse shaping for optical arbitrary pulse-train generation, J. Opt. Soc. Am. B **24**, 2124–2128 (2007).
[32] A. M. Weiner and D. E. Leaird, Generation of terahertz-rate trains of femtosecond pulses by phase-only filtering, Opt. Lett. **15**, 51–53 (1990).
[33] C. W. Hillegas, J. X. Tull, D. Goswami, D. Strickland, and W. S. Warren, Femtosecond laser pulse shaping by use of microsecond radio frequency pulses, Opt. Lett. **19**, 737–739 (1994).
[34] T. Brixner and G. Gerber, Femtosecond polarization pulse shaping, Opt. Lett. **26**, 557–559 (2001).
[35] M. Akbulut, R. Nelson, A. M. Weiner, P. Cronin, and P. J. Miller, Broadband polarization correction with programmable liquid-crystal modulator arrays, Opt. Lett. **29**, 1129–1131 (2004).
[36] M. Akbulut, A. M. Weiner, and P. J. Miller, Wideband all-order polarization mode dispersion compensation via pulse shaping, Opt. Lett. **30**, 2691–2693 (2005).
[37] L. Polachek, D. Oron, and Y. Silberberg, Full control of the spectral polarization of ultrashort pulses, Opt. Lett. **31**, 631–633 (2006).
[38] C. R. Menyuk, G. M. Carter, W. L. Kath, and R. M. Mu, in Optical Fiber Telecommunications, vol. IV B, I. P. Kaminow and T. Y. Li, Eds. San Diego: Academic Press, 2002.
[39] P. J. Winzer and S. Chandrasekhar, Return-to-zero modulation with electrically continuously tunable duty cycle using single NRZ modulator, Electron. Lett. **39**, 859–860 (2003).
[40] L.-S. Yan, S. M. R. M. Nezam, A. B. Sahin, J. E. McGeehan, T. Luo, Q. Yu, and A. E. Willner, Performance optimization of RZ data format in WDM systems using tunable pulse-width management at the transmitter, J. Lightwave Technol. **23**, 1063–1067, (2005).
[41] M. Matsuura, N. Kishi, and T. Miki, Widely pulsewidth-tunable multiwavelength synchronized pulse generation utilizing a single SOA-based delayed interferometric switch, IEEE Photonics Technol. Lett. **17**, 902–904, (2005).
[42] C. Yu, L. S. Yan, T. Luo, Y. Wang, Z. Pan, and A. E. Willner, Width-tunable optical RZ pulse train generation based on four-wave mixing in highly nonlinear fiber, IEEE Photonics Technol. Lett. **17**, 636–638, (2005).
[43] D. Norte and A. E. Willner, Experimental demonstrations of all-optical conversion between the RZ and NRZ data formats incorporating noninverting wavelength shifting leading to format transparency, IEEE Photonics Technol. Lett. **8**, 712–714, (1996).
[44] L. Xu, B. C. Wang, V. Baby, I. Glesk, and P. R. Prucnal, All-optical data format conversion between RZ and NRZ based on a Mach-Zehnder interferometric wavelength converter, IEEE Photonics Technol. Lett. **15**, 308–310, (2003).

[45] S. H. Lee, K. K. Chow, and C. Shu, Spectral filtering from a cross-phase modulated signal for RZ to NRZ format and wavelength conversion, Opt. Express **13**, 1710–1715, (2005).
[46] C.-B. Huang, Z. Jiang, D. E. Leaird, and A. M. Weiner, The impact of optical comb stability on waveforms generated via spectral line-by-line pulse shaping, Opt. Express **14**, 13164–13176 (2006).
[47] S. T. Cundiff, Phase stabilization of ultrashort optical pulses, J. Phys. D **35**, R43–R59 (2002).
[48] A. Bartels, R. Gebs, M. S. Kirchner, and S. A. Diddams, Spectrally resolved optical frequency comb from a self-referenced 5 GHz femtosecond laser, Opt. Lett. **32**, 2553–2555, (2007).
[49] S. Gee, F. Quinlan, S. Ozharar, and P. J. Delfyett, Simultaneous optical comb frequency stabilization and super-mode noise suppression of harmonically mode-locked semiconductor ring laser using an intracavity etalon, IEEE Photonics Technol. Lett. **17**, 199–201, (2005).
[50] M. Yoshida, T. Yaguchi, S. Harada, and M. Nakazawa, A 40 GHz regeneratively and harmonically mode-locked erbium-doped fiber laser and its longitudinal-mode characteristics, IEICE Trans. Electron. **E87C**,1166–1172 (2004).
[51] H. Murata, A. Morimoto, T. Kobayashi, and S. Yamamoto, Optical pulse generation by electrooptic-modulation method and its application to integrated ultrashort pulse generators, IEEE J. Sel. Top. Quantum Electron. **6**, 1325–1331, (2000).
[52] S. Hisatake, Y. Nakase, K. Shibuya, and T. Kobayashi, Generation of flat power-envelope terahertz-wide modulation sidebands from a continuous-wave laser based on an external electro-optic phase modulator, Opt. Lett. **30**, 777–779, (2005).
[53] K. Imai, M. Kourogi, and M. Ohtsu, 30-THz span optical frequency comb generation by self-phase modulation in an optical fiber, IEEE J. Quantum Electron. **34**, 54–60, (1998).
[54] Z. Jiang, C.-B. Huang, D. E. Leaird, and A. M. Weiner, Optical arbitrary waveform processing of more than 100 spectral comb lines, Nature Photonics **1**, 463–467 (2007).
[55] Z. Jiang, D. E. Leaird, and A. M. Weiner, Optical processing based on spectral line-by-line pulse shaping on a phase modulated CW laser, IEEE J. Quantum Electron. **42**, 657–665 (2006).
[56] C.-B. Huang, Z. Jiang, D. E. Leaird, and A. M. Weiner, High-rate femtosecond pulse generation via line-by-line processing of a phase-modulated CW laser frequency comb, Electron. Lett. **42**, 1114–1115 (2006).
[57] A. M. Weiner, D. E. Leaird, J. S. Patel, and J. R. Wullert, Programmable shaping of femtosecond optical pulses by use of a 128-element liquid crystal phase modulator, IEEE J. Quantum Electron. **28,** 908–920 (1992).
[58] S. X. Wang, S. J. Xiao, and A. M. Weiner, Broadband, high spectral resolution 2-D wavelength-parallel polarimeter for dense WDM systems, Opt. Express **13,** 9374–9380 (2005).
[59] M. Kourogi, K. Nakagawa, and M. Ohtsu, Wide-span optical frequency comb generator for accurate optical frequency difference measurement, IEEE J. Quantum Electron. **29**, 2693–2701 (1993).
[60] K. Imai, B. Widiyatmoko, and M. Kourogi, High finesse waveguide cavity optical frequency comb generator, Proceeding of 30th European Conference on Optical Communication (ECOC), We4.P.044 (2004).
[61] M. Kourogi, B. Widiyatmoko, K. Imai, and M. Ohtsu, Generation and application of an optical frequency comb, J. Commun. Res. Lab. **46**, 397–401 (1999).
[62] B. Widiyatmoko, K. Imai, M. Kourogi, and M. Ohtsu, Second-harmonic generation of an optical frequency comb at 1.55 μm with periodically poled lithium niobate, Opt. Lett. **24**, 315–317 (1999).
[63] Y. Bitou, T. R. Schibli, and K. Minoshima, Accurate wide-range displacement measurement using tunable diode laser and optical frequency comb generator, Opt. Express **14**, 644–654 (2006).
[64] G. M. Macfarlane, A. S. Bell, E. Riis, and A. I. Ferguson, Optical comb generator as an efficient short-pulse source, Opt. Lett. **21**, 534–536 (1996).
[65] M. Kato, K. Fujiura, and T. Kurihara, Generation of a superstable Lorentzian pulse train with a high repetition frequency based on a Fabry-Perot resonator integrated with an electro-optic phase modulator, Appl. Opt. **44**, 1263–1269 (2005).
[66] R. P. Kovacich, U. Sterr, and H. R. Telle, Short-pulse properties of optical frequency comb generators, Appl. Opt. **39**, 4372–4376 (2000).
[67] Z. Jiang, D. E. Leaird, C.-B. Huang, H. Miao, M. Kourogi, K. Imai, and A. M. Weiner, Spectral line-by-line pulse shaping on an optical frequency comb generator, IEEE J. Quantum Electron. **43**, 1163–1174 (2007).
[68] E. Frumker and Y. Silberberg, Femtosecond pulse shaping using a two-dimensional liquid-crystal spatial light modulator, Opt. Lett. **32**, 1384–1386 (2007).
[69] C. W. Hillegas, J. X. Tull, D. Goswami, D. Strickland, and W. S. Warren, Femtosecond laser pulse shaping by use of microsecond radio-frequency pulses, Opt. Lett. **19**, 737–739 (1994).
[70] E. Frumker, E. Tal, Y. Silberberg, and D. Majer, Femtosecond pulse-shape modulation at nanosecond rates, Opt. Lett. **30**, 2796–2798 (2005).
[71] S. Ozharar, F. Quinlan, S. Gee, and P. J. Delfyett, Demonstration of endless phase modulation for arbitrary waveform generation, IEEE Photonics Technol. Lett. **17**, 2739–2741 (2005).
[72] S. Ozharar, S. Gee, F. J. Quinlan, and P. J. Delfyett, Time-division-multiplexing-based modulation scheme for RF chirp extension, Electron. Lett. **42**, 714–715 (2006).
[73] D. E. Leaird, Z. Jiang, and A. M. Weiner, Experimental investigation of security issues in OCDMA: a code-switching scheme, Electron. Lett. **41**, 817–819 (2005).
[74] P. J. Delfyett, S. Gee, C. Myoung-Taek, H. Izadpanah, L. Wangkuen, S. Ozharar, F. Quinlan, and T. Yilmaz, Optical frequency combs from semiconductor lasers and applications in ultrawideband signal processing and communications, J. Lightwave Technol. **24**, 2701–2719 (2006).
[75] J. D. McKinney, D. E. Leaird, and A. M. Weiner, Millimeter-wave arbitrary waveform generation with a direct space-to-time pulse shaper, Opt. Lett. **27**, 1345–1347 (2002).
[76] I. S. Lin, J. D. McKinney, and A. M. Weiner, Photonic synthesis of broadband microwave arbitrary waveforms applicable to ultra-wideband communication, IEEE Microw. Wirel. Compon. Lett. **15**, 226–228 (2005).
[77] C.-B. Huang, D. E. Leaird, and A. M. Weiner, Time-multiplexed photonically enabled radio-frequency arbitrary waveform generation with 100 ps transitions, Opt. Lett. **32**, 3242–3244 (2007).

